Journal of Medicinal Chemistry

pubs.acs.org/jmc

Article

Fragment-Based Covalent Targeting of Lysines at the Allosteric Latch Site of SHP2

Vincenzo Di Lorenzo, Noémi Csorba, Renáta Szabó, Levente Kollár, Yvette Roske, Ivan Radelović, Krisztina Balázs, Tibor Viktor Szalai, Nina-Louisa Efrém, Levente Mihalovits, Tímea Imre, József Simon, József Tóvári, Marc Nazaré, Oliver Daumke, Péter Ábrányi-Balogh,* and György M. Keserű*

Cite This: https://doi.org/10.1021/acs.jmedchem.6c01030

Read Online

ACCESS | Metrics & More | Article Recommendations | Supporting Information

ABSTRACT: Covalent mechanism of action is a powerful way to modulate challenging drug targets. Here, we present a streamlined workflow that combines covalent fragment screening (electrophile first approach) and ligand-first strategy to identify covalent inhibitors targeting lysine residues in the allosteric latch site of SHP2 phosphatase. Supported by complementary computational and experimental analyses, this strategy enabled us to identify the first potent cell active allosteric covalent inhibitors acting at this site. Demonstrating the covalent tractability of the latch site opens further avenues for future optimization and therapeutic exploration of high-value allosteric SHP2 inhibitors.

KEYWORDS: *SHP2 phosphatase, covalent inhibitor, allosteric modulator, lysine labelling, NHS-ester, dichlorotriazine, X-ray structure*

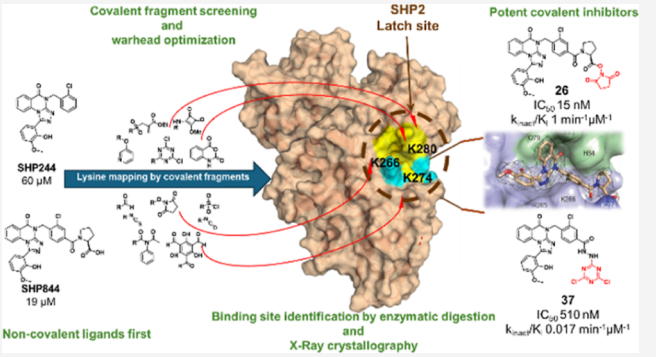

INTRODUCTION

SHP2 (Src homology 2-containing protein tyrosine phosphatase 2) is a non-receptor tyrosine phosphatase that is allosterically regulated and has clinical relevance as an anticancer drug target.[1,2] SHP2 plays a central role in receptor tyrosine kinase (RTK) signaling, and its activation can lead to oncogenic processes via Ras/Raf/ERK and PI3K/AKT signaling pathways.[3,4] SHP2 is also involved in the evasion of the immune response of tumor cells through programmed cell death receptor signaling in T cells and the resulting alteration of the tumor microenvironment. Aberrant SHP2 activation has been shown to promote the progression of different cancer types including hematologic cancers and solid tumors.[2] Its diverse role in multiple signaling pathways positions SHP2 as an important target to overcome drug resistance of kinase inhibitors and programmed cell death-1 (PD-1) blockade.[5] Although the importance of SHP2 in drug resistance and tumor progression has long been recognized, it is considered a challenging drug target, like other protein tyrosine phosphatases.[3,6] This paradigm is slowly changing since the discovery of allosteric SHP2 inhibitors, which have improved drug-like properties compared to orthosteric inhibitors and successfully reached clinical trials.[5,6]

SHP2 contains two Src homology 2 domains (N-SH2 and C-SH2), the highly conserved protein tyrosine phosphatase (PTP) domain harboring the orthosteric site and a flexible C-terminal tail. There are three less conserved allosteric sites participating in the unique allosteric regulation of SHP2 and enabling opportunities to design selective and potent SHP2 inhibitors. In particular, the "tunnel" allosteric site at the C-SH2/PTP domain interface, the "latch" site, located at the N-SHP2/PTP domain interface, and the "groove" site that resides on the opposite side of the "tunnel" site.[7] The tunnel and latch allosteric sites have distinct and complementary regulatory roles in controlling SHP2 catalytic activity, therefore both can be considered for targeting.[8] Up to now, however, all advanced allosteric inhibitors act at the tunnel allosteric site of SHP2. No other pocket, including the latch site, has been targeted with similarly potent compounds.[5,8−10]

The covalent mechanism of action became an important modality targeting enzymes and challenging targets[11−15] such as transcription factors,[16−18] GTPases[19−22] and E3 ligases.[23−26] In the last decades, targeted covalent inhibitors (TCIs) and covalent binders engaged mostly cysteines. However, the availability of new warheads against further nucleophilic amino acids enabled labelling serine, tyrosine and lysine residues.[12,27−31] Targeting non-cysteine residues has made many human proteins amenable for covalent intervention. Out of the other residues,

Received: March 31, 2026
Revised: August 14, 2026
Accepted: August 21, 2026

lysines are three times as abundant as cysteines, located at functionally relevant positions in many targets, and provide specific binding options for electrophiles in cavities that protect them from protonation. In fact, a chemoproteomic study revealed more than 14,000 tractable lysines in the proteome of MDA-MB-231 and Ramos cells, out of which at least 3000 were potentially druggable, with a small library of electrophilic fragments.[32] Our aim in the present study was therefore to identify tractable lysine residues at allosteric SHP2 sites using fragment electrophiles that have higher probabilities for identifying such pockets. Chemoproteomic studies identified only a single tractable lysine (K496) in SHP2,[32] however, our previous approach targeting the tunnel site with target-specific covalent fragments[33] and our positive experience in mapping the reactivity and accessibility of cysteines[34,35] prompted us to develop a similar approach to identify further lysines for covalent labeling. Consequently, we compiled a 35-membered fragment set representing 25 lysine-reactive warheads and screened the library as an electrophile first approach against SHP2. Next, we identified the labelling site of the most promising fragments, revealing tractable lysine residues at both the tunnel and the latch allosteric sites. Given the lack of highly potent inhibitors acting on to the latch site, we focused our efforts on this site and initiated a ligand-first approach combining warheads labelled lysines at the latch site with latch-targeting reversible SHP2 inhibitors.

Considering known reversible latch site SHP2 ligands, our attention turned to Novartis compounds **SHP244**, **SHP504** and **SHP844** (Figure 1A).[36] **SHP244** has been identified as a HTS (high-throughput screening) hit screened against $SHP2^{1-525}$ (containing N-SH2, C-SH2 and PTP domains) with an IC_{50} of 60 μM.[36] X-ray crystallography (PDB 6BMR) revealed that this compound stabilizes the inactive, closed conformation of SHP2 when bound to the latch site (Figure 1B). Analysis of ligand−protein interactions revealed that the chlorophenyl and the triazoloquinazolinone rings of **SHP244** accommodate at a hydrophobic groove that terminates in hydrophilic residues including K266, K274 and K280.[36] Therefore, **SHP244** has been extended by a carboxyl group to form polar interactions with K266 and K280, which resulted in **SHP504** ($SHP2^{1-525}$ IC_{50} 21 μM) and **SHP844** ($SHP2^{1-525}$ IC_{50} 18.9 μM), respectively. Their binding modes were confirmed by X-ray crystallography (Figure 1B), showing salt bridge interactions between the carboxyl group of **SHP504** (6BMV) and **SHP844** (6BMX) and K266 and K280, respectively.[36] Despite of the extensive exploration of the SAR around these compounds, efforts to increase the potency were unsuccessful and it was concluded that "further considerations are necessary to find potent latch inhibitors".[37−39]

Given the close proximity of tractable lysine resides around the Novartis compounds, we equipped the most efficient lysine warheads identified at the latch site to their 4-(2-chlorobenzyl)-1-aryl-[1,2,4]triazolo[4,3-*a*]quinazolin-5(4*H*)-one core and characterized the corresponding derivatives in biophysical and biochemical assays. This combination of electrophile-first warhead screening and ligand first design led to the identification of the first submicromolar covalent allosteric inhibitors of SHP2 acting at the underexplored latch site.

RESULTS AND DISCUSSION

Screening the Lysine Reactive Mapping Library—Electrophile First Approach

As the first step of our strategy, we compiled a 35-membered library of lysine-reactive fragments comprising 25 diverse aminophilic warhead chemotypes to map the available Lys residues on SHP2, particularly at the latch allosteric site. This set of electrophiles was selected from known covalent warheads and small molecules described for targeting lysine residues in covalent fragment, targeted covalent inhibitor or activity-based proteomics profiling studies (see Supporting Information for the structure and warhead-types (Figure S1, Table S1).[27,32,40−42]

Lysine reactivity of the library members was first tested in a kinetic assay using excess *N*-α-acetyl lysine.[27] Reaction kinetics were measured for 24 h, and the consumption of the electrophilic fragments was followed by HPLC-MS (Table S2).[43−45] Half-lives ($t_{1/2}$) and pseudo-first-order rate constants (k_{Lys}) revealed that the library covers a wide range of intrinsic reactivities that qualified it for mapping tractable lysine residues with diverse nucleophilicity.[41]

Next, the library was screened in a DiFMUP-based chromogenic biochemical assay developed in-house against full-length SHP2 to identify those fragments that are functionally active against SHP2. In this assay, SHP2 is allosterically activated upon binding of a *bis*-tyrosyl-phosphorylated IRS-1-derived peptide to its SH2 domains, which results in the disruption of its autoinhibitory interface. This conformational change activates the PTP domain, enabling substrate recognition and catalysis, and thus allows the assay to capture various modes of phosphatase inhibition using DiFMUP as the substrate.[4,36] In a single dose screening at 100 μM concentration, 26 fragments showed >50% inhibition (Table S1). IC_{50}s were determined for the most active compounds with 12 of 26 exhibiting IC_{50}s below 100 μM (Figure S5, S6). These hits were further investigated to prove covalent labelling of SHP2 by intact protein LC−MS followed by tryptic digestion and LC−MS/MS analysis (Figure S2, Table S2).

SHP2 contains 32 lysines, among which 10 were labelled. K492 and K280 located at the allosteric tunnel and latch sites were labelled by five and six fragments, respectively (Figure S2 and Table S2). Our further attention was focused on the most active covalent binders labelling lysine residues at the latch site (K266, K274 and K280, Figure 2). These lysines have comparable intrinsic reactivities (virtually identical nucleophilicity) and K274 and K280 showed similar accessibility as approximated by the calculated pK_a values (pK_a^{calcd} 10.1−10.4, computed by Propka Module by Schrödinger[46−48] using crystal structure 6BMX[35]) and by the calculated solvent accessible surface area (SASA) (83.7−87.3 Å^2), respectively. The accessibility of K266 was predicted to be somewhat better (SASA = 137.2 Å^2). Despite its higher predicted accessibility, no labelling was detected at K266.

Labelling of the latch site was detected with four warhead chemotypes including *N*-alkyl-*N*-aryl sulfonamide (NASA, **F8**), isatoic anhydride (**F15**), and dichlorotriazine (**F17**) labeling K280. NHS-esters (**F10-12**) showed different reactivity towards the lysines located at the latch site: **F12** labelled only K280 while the two smaller compounds (**F10** and **F11**) could bind to K274 as well (Figure 2). Considering labelling chemistries, fragment hits react mostly through acylation (**F8, F10-12, F15**) and the dichlorotriazine (**F17**) through aromatic nucleophilic substitution (S_NAr). Finally, covalent docking was performed to

https://doi.org/10.1021/acs.jmedchem.6c01030
J. Med. Chem. XXXX, XXX, XXX−XXX

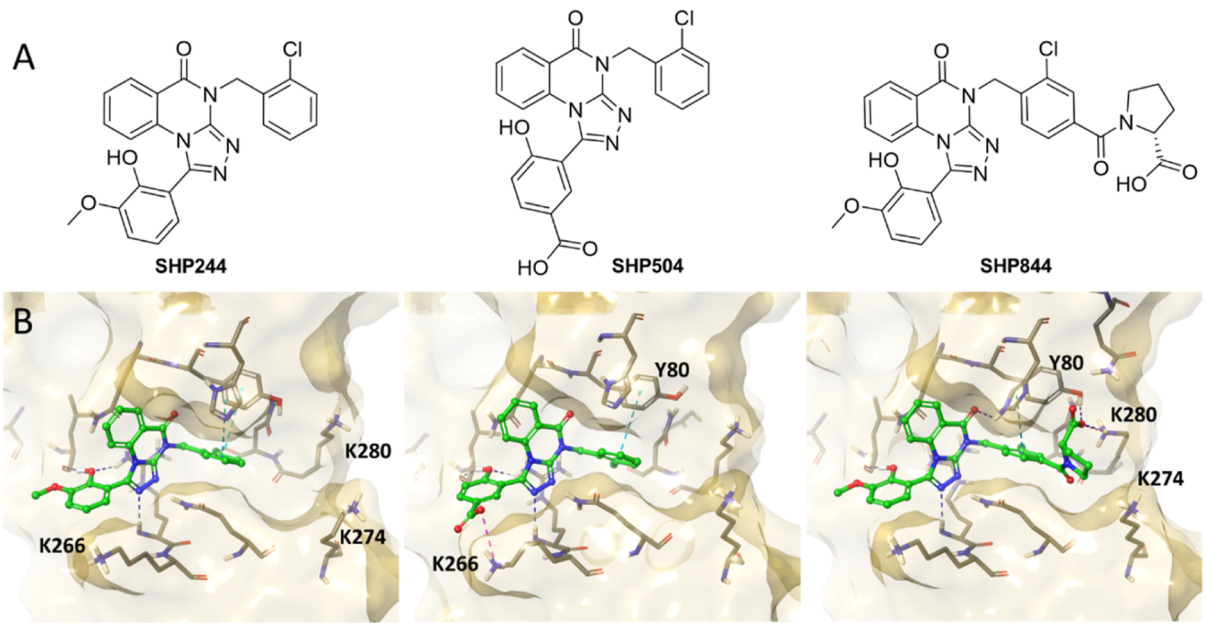

Figure 1. A: Chemical structures of **SHP244**, **SHP504** and **SHP844**. **B**: Latch site SHP2 inhibitors with experimental binding modes (from left to right: SHP244 (PDB 6BMR), SHP504 (PDB 6BMV) and SHP844 (PDB 6BMX)), highlighting important residues and protein−ligand interactions. Protein−ligand interactions are highlighted as dashed lines, with dark blue coloring corresponding to hydrogen bonds, cyan coloring corresponding to pi−pi interactions, and magenta coloring corresponding to salt bridges.

investigate protein interactions of the hits. Docking results showed that all fragments fit well within the binding site (Figure 2A−C). The *bis*(trifluoromethyl)benzene moieties adopted similar predicted poses in **F8**, **F10**, and **F17** (Figure 2A), and nearly identical predicted poses in **F11** and **F15** (Figure 2B). In the case of **F12**, the chromene moiety occupies the same sub pocket as the appropriate aromatic moieties in the other fragments. Its benzene ring located identical to that of the aromatic moieties in **F11** and **F15**, and the pyran ring occupied similar location to that of the aromatic rings in **F8**, **F10** and **F17** (Figure 2C). Overall, the location of the aromatic scaffolds in all fragments are spatially conserved within the pocket.

Design of SHP244, SHP504 and SHP844 covalent analogues—ligand first approach

Based on the mapping results and the known binding modes of triazoloquinazolinone latch inhibitors, we aimed to explore the three potential exit vectors of the **SHP244**, **SHP504** and **SHP844** cores using the most efficient NHS ester warhead. In this effort, the tractability of lysines at this site was assessed by combining non-covalent and covalent docking with SAR-based design considerations. All synthesized compounds were designed to retain the core 4-(2-chlorobenzyl)-1-aryl-[1,2,4]triazolo[4,3-*a*]quinazolin-5(4*H*)-one motif, preserving key non-covalent interactions while allowing scaffold-dependent projection of the warhead toward lysine side chains of interest.

SHP504 derivatives (compounds **12** and **13**), were designed to target K266 and showed minimal perturbations in their binding mode relative to the parent molecule, (MCS-RMSD 0.103−0.411 Å), suggesting that removal of the *ortho*-OH on ring D was unlikely to alter their interactions substantially (Figure 3). Covalent docking further indicated that this modification may improve K266 access to the NHS ester and facilitate covalent engagement turning the reversible Novartis ligands into a covalent inhibitor (Figure S3A).

The synthesis of the inhibitors followed literature procedures.[36,49] First, we synthesized the two carboxylic acids **10** and **11** and their NHS ester derivatives **12** and **13** (Scheme 1). In brief, 2-chlorobenzlyamine (**2**) was acylated with isatoic anhydride (**1**), followed by a cyclic thiourea formation using CS_2. Thiourea **4** was transformed to hydrazone **5**, and then *bis*-hydrazones (**8,9**) were synthesized by adding the corresponding formylbenzoic acids. The triazole ring was closed using $FeCl_3$ leading to **10,11**. For these latter steps, we found that using the appropriate concentration (0.5 M) and reaction temperatures were critical (for further information see Supporting Information). The targeted NHS esters (**12,13**) were then obtained by DCC-mediated acylation of *N*-hydroxysuccinimide.

NHS esters **12** and **13** were then tested against SHP2 showing low micromolar potency (IC_{50} 4.3 μM and 7.9 μM, respectively, Figure S7, Table 1) and clear labelling in intact MS. Their activity can be rationalized by docking results, as both adopt a similar predicted binding pose (Figure S3A). Unfortunately, digestions with different enzymes were unsuccessful to produce a K266-containing peptide suitable to confirm its labeling by MS-based mapping. Our peptide mapping and intact MS data, however, indirectly suggests K266 labelling since we did not observe modification at the other two accessible lysines (K274 and K280). Some remaining activity was observed for the non-covalent analogues **10** and **11** (IC_{50} 299 μM and 214 μM, respectively, Figure S6, Table 1). Comparison of **10** (*meta*-COOH) with **SHP504** points at pivotal effect of the *ortho*-hydroxyl group of **SHP504** enhancing the activity in line with reported SAR on this ring.[37] Since ring D was heavily sampled in previous SAR studies[37,38] with no significant success, our further efforts focused on other regions of the core. In conclusion, comparing the activity of SHP504 (IC_{50} 21 μM) with NHS esters **12** and **13**, this attempt of the ligand-first strategy provided 3-5 fold improvement in potency.

Next, we investigated the modification of **SHP244** and **SHP844**. For the **SHP844** NHS-ester derivative, non-covalent

https://doi.org/10.1021/acs.jmedchem.6c01030
J. Med. Chem. XXXX, XXX, XXX−XXX

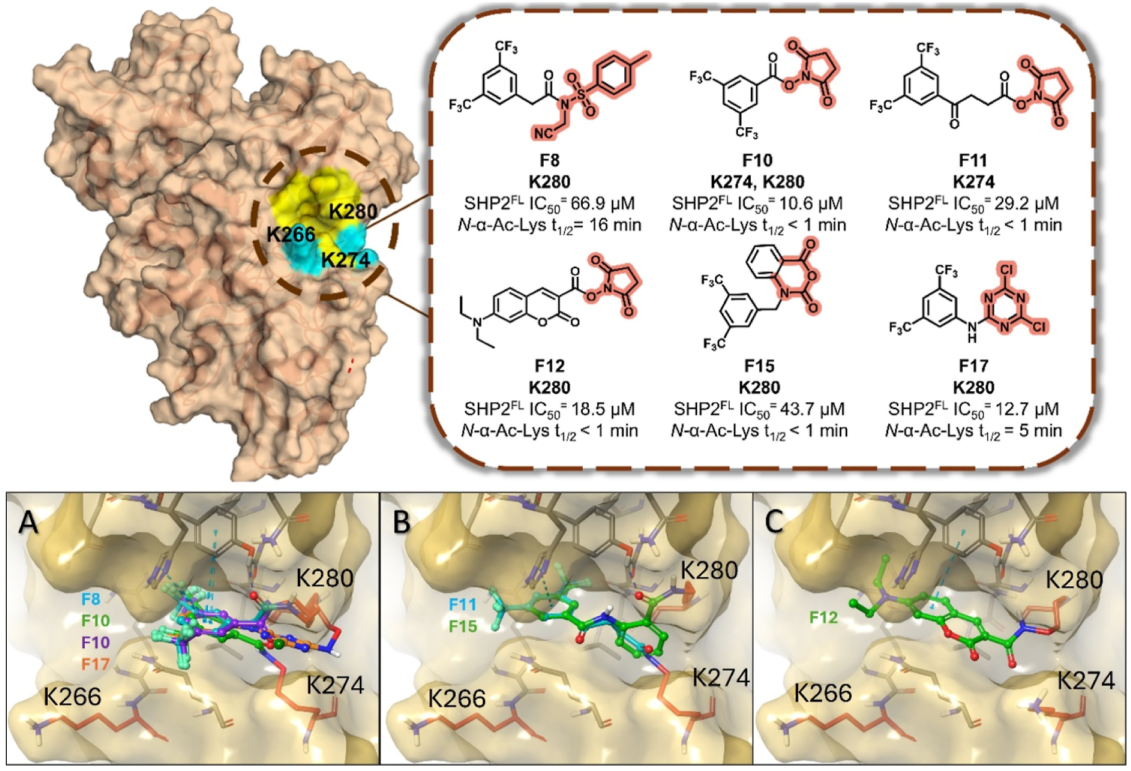

Figure 2. Latch-site reactivity profiling of the lysine-targeting covalent fragment library. Targetable lysines (cyan coloring) of the allosteric latch site of SHP2 (PDB 6BMX) highlighted with yellow. *N*-α-acetyl lysine reactivity ($t_{1/2}$, h), IC_{50} values and the labeled lysine residues of the most potent hit fragments are shown alongside their chemical structures, with the warheads highlighted in red. Panels (A–C) show the predicted best scoring binding poses resulted from covalent docking (PDB: 6BMX). Ligands with similar binding poses are presented on the same panel, with targeted residues (K274 and K280) colored red, and interactions showed as dashed lines, with light blue color corresponding to $\pi-\pi$ stacking, and dark blue color corresponding to hydrogen bond. (A): **F10** binding to K274 (colored green), **F8** binding to K280 (colored cyan), **F10** binding to K280 (colored purple) and **F17** binding to K280 (colored orange). **B**: **F15** binding to K280 (colored green) and **F11** binding to K274 (colored cyan). **C**: **F12** binding to K280.

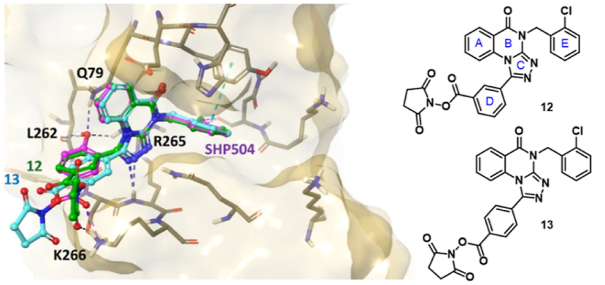

Figure 3. Predicted binding modes from docking for **SHP504** NHS-ester analogues modified at meta (**12**) or para (**13**) positions of ring D (green and light blue, respectively) (PDB 6BMV) and their chemical structures. **SHP504** reference colored in magenta.

docking predicted hydrogen bonds between the NHS moiety and K274, K280, and Y80 that could help to orient the active ester for nucleophilic attack (Figure 4A). Non-covalent docking of the **SHP244** series identified position 4 of the chlorobenzyl substituent as the preferred site for NHS installation (Figure 4B). Although the NHS carbonyl is further from K274 and K280 in docked poses, elevated *B*-factors for these lysine side chains (in PDB entries 6BMR, 6BMX, 6BMY, 6BMU and 6BMV) suggest that their conformational mobility could allow transient proximity of the lysine ε-amino groups to the NHS carbonyl and enable covalent capture. Covalent docking suggested that the K274 and K280 side chains might be flexible enough to reach the electrophile without disturbing the non-covalent interactions of the scaffold (Figure S3B). Consequently, docking calculations confirmed the feasibility of this strategy to provide covalent inhibitors by the functionalization of the proline or modification of ring E to target K274 or 280.

The synthesis of these analogues was started by the preparation of thiourea **15**, the 4-methoxybenzyl derivative of **4** (Scheme 2). The synthesis followed similar steps as described above, and the protecting group was removed after the formation of the TIPS-protected triazole **19**. The carboxylic acid derivative of **SHP244** (**23**) was formed from precursors **21** or **22** by hydrolysis after the alkylation of intermediate **20** using the corresponding benzonitrile or methyl benzoate.

Then, the resulting carboxylic acid (**23**) was reacted with both proline enantiomers leading to the two enantiomeric carboxylic acids (**24**,**25**) that were converted to the corresponding NHS-esters (**26**,**30**) or other electrophilic derivatives (**27**–**29**) (Scheme 3). In addition, the NHS-ester derivative (**31**) of **23** was also isolated.

Compound **31** did not show significantly improved activity (IC_{50} 28 μM, Figure S9, Table 1) compared to SHP244 (IC_{50} 60 μM) or SHP844 (IC_{50} 18.9 μM).[36] This finding was consistent with the calculated suboptimal pre-reaction geometry and the long distance between the warhead and K274 or K280, as seen in docking simulations (Figure 4B). However, its non-covalent analogue (**23**) exhibited unexpectedly strong inhibition (IC_{50} 4.1 μM, Figure S8, Table 1) similar to its methyl ester

https://doi.org/10.1021/acs.jmedchem.6c01030
J. Med. Chem. XXXX, XXX, XXX–XXX

Scheme 1. Synthesis of SHP504 Analogue Acids 10,11 and NHS-Esters 12,13

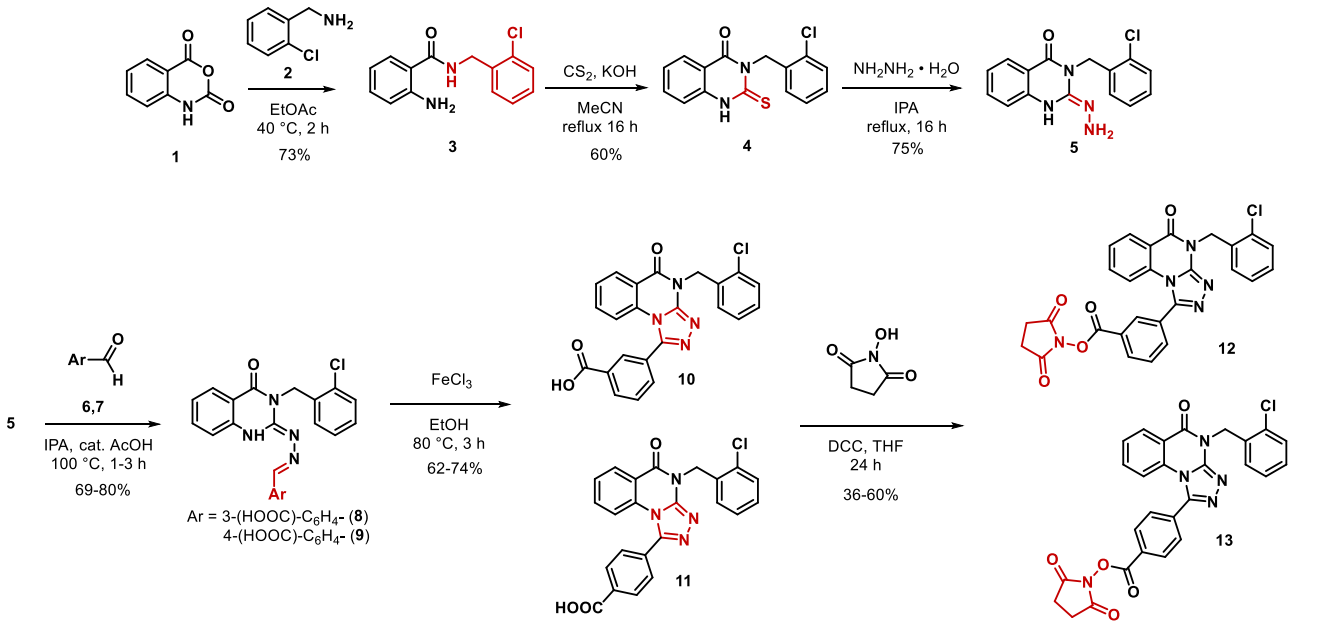

Table 1. Biological Activity for the Synthesized Non-covalent and Targeted Covalent Inhibitors

compound	inhibition % or IC_{50}	compound	inhibition % or IC_{50}
10	299 ± 39 μM	**27**	25.1 ± 5.3 μM
11	214 ± 27 μM	**28**	12% @ 10 μM
12	4.3 ± 0.5 μM	**29**	4.5 ± 1.0 μM
13	7.9 ± 0.5 μM	**30**	0.94 ± 0.24 μM
21	57.3 ± 20.3 μM	**31**	28.0 ± 3.3 μM
22	3.1 ± 0.7 μM	**34**	41.0 ± 3.4 μM
23	4.1 ± 0.2 μM	**35**	15.6 ± 1.6 μM
24	21.6 ± 3.5 μM	**36**	677 ± 180 μM
25	0% @ 10 μM	**37**	0.51 ± 0.08 μM
26	15.0 ± 2.3 nM		

(**22**) that was particularly active (IC_{50} 3.1 μM, Figure S8, Table 1). This suggests that the loss of activity in **31** could be related to the NHS-moiety that might prevent forming non-covalent interactions.

Next, the carboxylic acid available on the proline side chain of **SHP844** was converted to the corresponding NHS ester. (*S*)-**SHP844**-NHS (**26**) enabled acylation of K274 yielding a marked increase in potency (IC_{50} of 15 nM, Figure S9, Table 1), thereby establishing **26** as the most potent compound of the series. The other (*R*)-proline enantiomer (**25**) was also investigated but compared to its progenitor showed no inhibition at 10 μM (Figure S9, Table 1); however, its NHS ester (**30**) exhibited substantially increased activity (IC_{50} 0.9 μM, Figure S9, Table 1). These results demonstrate that covalent activation might produce considerable gains in inhibitory potency. The interactions formed in the covalent complex of the most potent compound **26** at the latch site of SHP2 were explored by X-ray crystallography (Figure 5). Human $SHP2^{2-525}$ was co-crystallized with compound **26**, yielding crystals which diffracted to 2.6 Å. The determined SHP2 structure showed a well-defined electron density for compound **26**, confirming its covalent binding (Figure 5A) and clearly providing its orientation in the binding site (Figure 5A inset).

Detailed inspection of the structure revealed that Q79, L262, R265 of SHP2 form hydrogen bonds to the hydroxy group of the 2-hydroxy-3-methoxyphenyl, whereas N1 of the 1,2,4-triazole ring interacts via H-bonds with R265 and Q269. Hydrophobic interactions of Q79, E83, L283 as well π-cation (K283) and π-stacking (Y80) interactions to the central triazoloquinazolinone and the 3-chlorophenyl, respectively, stabilized the binding of **26** in the allosteric site (Figure 5B). Comparing the binding of compound **26** with the related **SHP844** (PDB: 6BMX) by superimposition revealed a striking ~180° rotation of the proline ring, with the associated carboxyl group covalently binding to K274 (Figure 5C).

To find explanation for the activity difference of **26** and **30**, we first compared the predicted non-covalent binding modes of carboxylic acid **24** and **25**, which showed only slight differences in the proline substructure (Figure 6A). Covalent docking to residue K274 showed similar results, as the flexibility of the labelled residue allowed similar binding poses for both **26** and **30**. The non-covalent docking of NHS esters **26** and **30** interestingly showed that contrary to **26**, **30** was unable to fit into the latch site (Figure S3C,D). This indicates that **30** might not be able to fit into the binding site easily explaining its reduced activity. Importantly, covalent activation (as exemplified by compound **30**) can mitigate this loss of activity by enabling covalent capture despite suboptimal pocket complementarity.

Although (*S*)-**SHP844**-NHS (**26**) ester provided the proof of concept for our covalent allosteric approach at the latch site of SHP2, its high reactivity prompted us to test other active esters (Table S3). The simple phenyl ester (**28**) was essentially inactive (12% inhibition at 10 μM), the pentafluorophenyl ester (**27**) showed modest activity (IC_{50} 25 μM, Figure S9, Table 1), and the pyridine-3-yl ester (**29**) was the most active non-NHS ester (IC_{50} 4.5 μM, Figure S9, Table 1) with ~90% single labelling by intact-protein MS. Our docking analysis revealed that the pentafluorophenyl substituent of compound **27** fails to form complementary contacts with nearby residues. In addition, its inability to fit into the binding site likely renders this hydrophobic moiety solvent exposed,

https://doi.org/10.1021/acs.jmedchem.6c01030
J. Med. Chem. XXXX, XXX, XXX−XXX

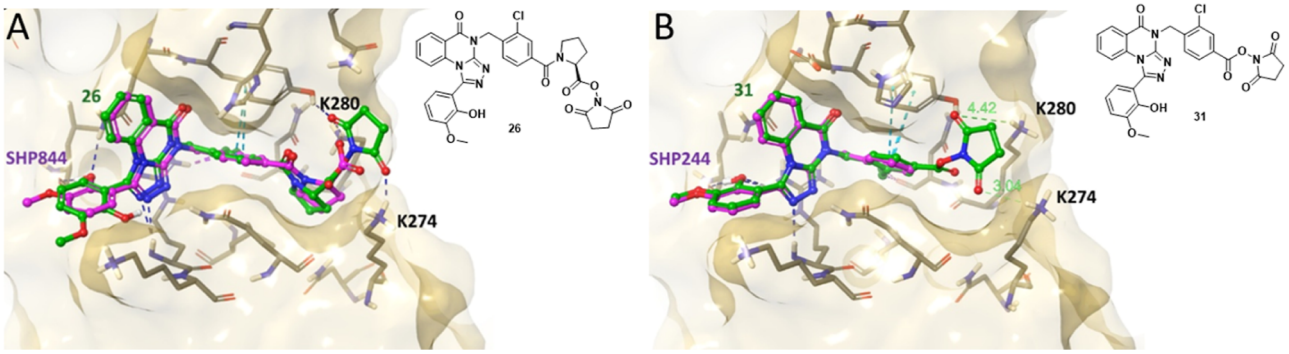

Figure 4. (A): Predicted binding mode and chemical structure of **SHP844** NHS-ester analogue (**26**, colored in green) (PDB 6BMX). **SHP844** reference colored in magenta. (B): Predicted binding mode and chemical structure of **SHP244** NHS-ester analogue (**31**, colored in green) (PDB 6BMR), with the distances between the NHS group and K274/K280 shown with green label (4.42 Å from K280, 3.04 Å from K274). **SHP244** reference colored in magenta. Interactions are shown as dashed lines, with light blue coloring corresponding to $\pi-\pi$ stacking, dark blue coloring corresponding to hydrogen bond and purple coloring corresponding to halogen bonds.

Scheme 2. Synthesis of Key Intermediates 22 and 23

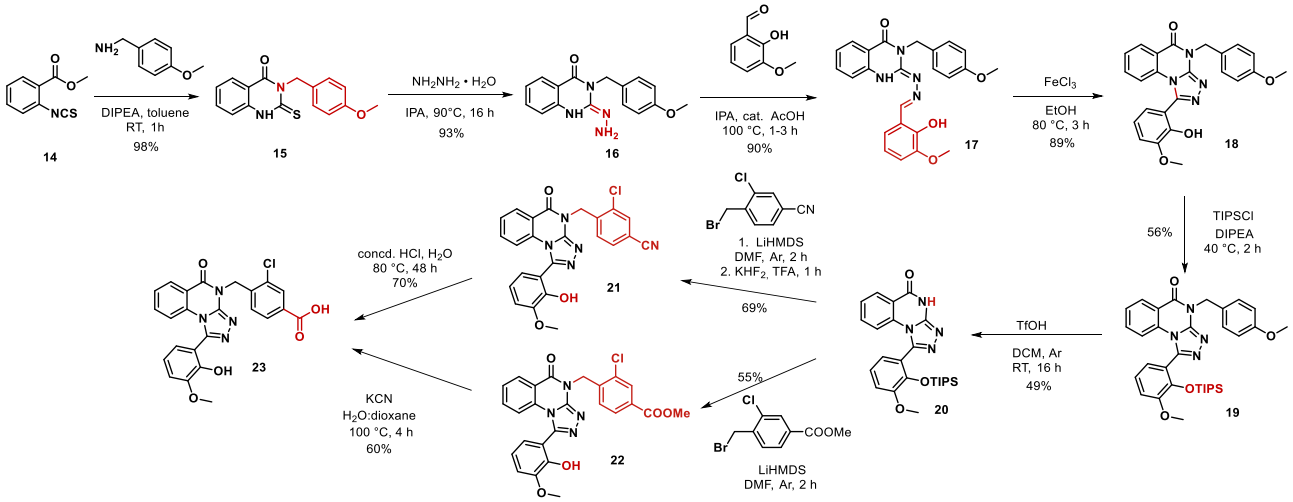

Scheme 3. Synthesis of SHP844 Analogues

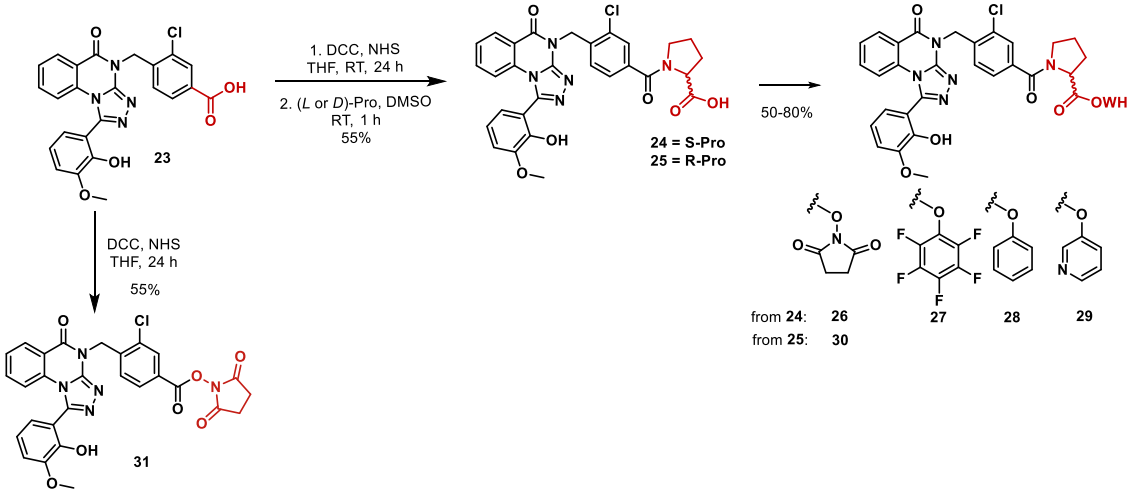

which likely accounts for its reduced activity (Figure 6C). Compounds **28** and **29** show essentially identical binding modes (MCS-RMSD 0.085 Å), with the phenyl or pyridine-3-yl group located in a solvent-exposed region (Figure 6D). As the binding site contains mostly polar residues in that region (Q87, Y80, K274, K280, N281) the difference in activity could be rationalized by lacking polar contacts of the hydrophobic phenyl ring in **28**.

https://doi.org/10.1021/acs.jmedchem.6c01030
J. Med. Chem. XXXX, XXX, XXX–XXX

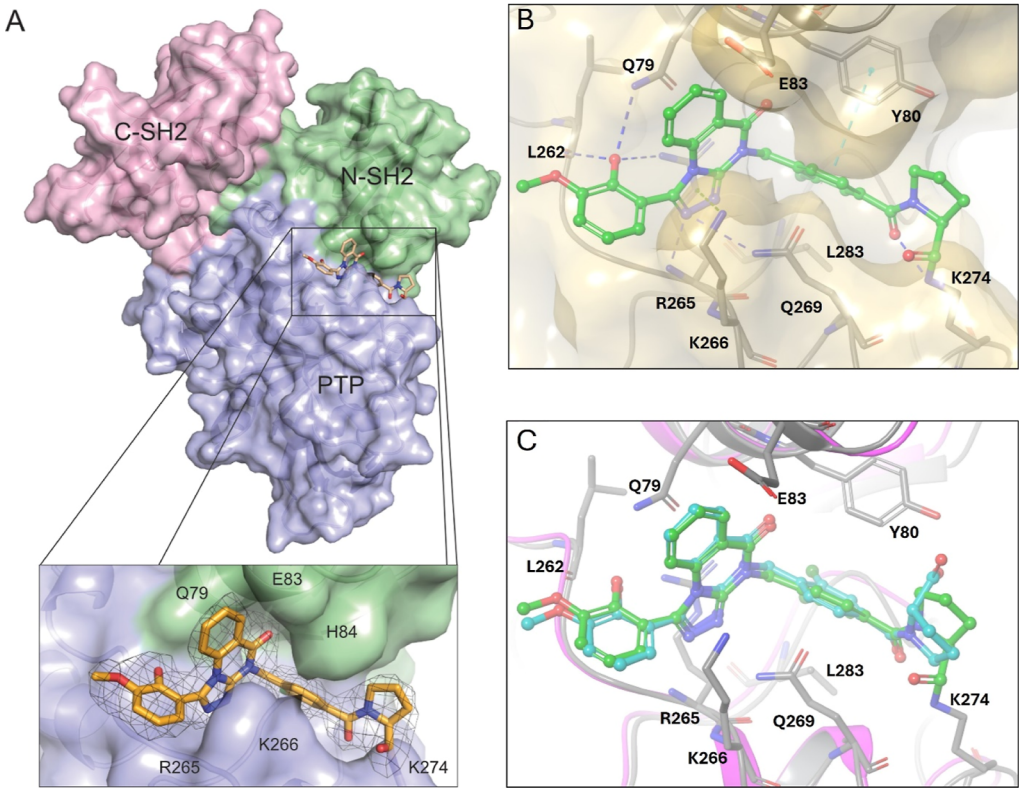

Figure 5. X-ray structure of SHP2 with covalently bound compound **26** (PDB: 29CY). (A): Surface presentation of SHP2 with colored N-terminal, C-terminal SH2 and PTP domain in green, magenta, blue, respectively. The inset shows the latch allosteric site with covalently bound compound **26** (orange) surrounded by well-defined electron density depicted as mesh at a contour-level of 1.0 sigma. (B): Detailed representation of interactions of compound **26** (green) with SHP2 shown as dashed lines with H-bonds highlighted in blue, π-cation interaction in green and π-stacking interaction in cyan. (C): Superimposition of SHP2 with **SHP844** (PDB: 6BMX, in magenta) in light blue onto compound **26**-bound SHP2 in green.

Comparing the activity of the non-covalent analogues to that of the covalent **31** suggested further optimization of the warhead vector or its linker. Therefore, we explored further linking strategies and covalent warheads with alternative labelling mechanisms. Covalent fragment screening and subsequent docking simulations suggested the dichlorotriazine warhead (**F17** fragment) as a viable option tackling lysines in the latch site through an S_NAr reaction. The installation of this warhead was achieved through three linkers using NHS-ester **31** and methyl ester **22** as key intermediates. These acylated either aniline (**32**), ethylenediamine (**33**), or hydrazine (**36**) linkers[50] that were next equipped with the dichlorotriazine warhead in S_NAr reactions leading to inhibitors **34**, **35** (Scheme 4A) and **37** (Scheme 4B), respectively. When designing compound **34**, the *meta* position of the aromatic linker was suggested to be suitable by non-covalent docking (Figure S4).

The larger aniline or the longer but flexible ethylenediamine linkers provided inhibitors **34** and **35** with IC_{50}s 41 μM and 16 μM, respectively (Figure S10, Table 1). However, when we applied a short hydrazide linker, covalent inhibitor **37** showed an IC_{50} of 0.51 μM (Figure S10, Table 1), which represented the second most potent compound in the series labelling K280, as proven by enzymatic digestion. Non-covalent docking of **34**, **35** and **37** suggest that their dichlorotriazine groups are in a solvent-exposed region. Despite that, it can establish hydrogen bond with N281 in **37**, anchoring it to the edge of the latch site and projecting the reactive chlorine into proximity of the lysine ϵ-amino groups. This orientation is geometrically poised for nucleophilic aromatic substitution (S_NAr) while still maintaining favorable non-covalent contacts. In contrast, the dichlorotriazine group of **34** and **35** moves towards Q271 and R270 on the protein surface that creates larger solvent-exposed areas, which could explain their lower activity (Figure 7A). Covalent docking confirmed that longer linkers (in case of **34** and **35**) move the dichlorotriazine group farther from the latch site and the larger solvent-exposed regions reduce their activity (Figure 7B). The loss of activity observed for the non-covalent precursor hydrazide of **37** (**36**, $IC_{50} = 677$ μM, Figure S8, Table 1) highlights the key role of the covalent interaction. In fact, comparing the non-covalent precursors, all three compounds (**22**, **23** and **36**) established a hydrogen bond with K280. However, the larger polar surface area likely increases the desolvation penalty upon binding, which, together with the constrained scaffold orientation (due to interaction with K280), might explain the reduced potency of **23** and **36**. The salt bridge interaction of **23** with K274 partially compensates this penalty (Figure 7C).

Collectively, E-ring modifications yielded both non-covalent and covalent compounds with remarkable activity achieving >40−400 fold improvement compared to **SHP244** or **SHP844** identifying it as a promising and underexplored site for further optimization (Table 1).

We then determined k_{inact} and K_I values[51] of the best-performing compounds (NHS ester **26** and dichlorotriazine **37**) by time-dependent IC_{50} measurements (Figure 8, Table S4).[52] The k_{inact} values revealed similar reactivity for the two inhibitors (0.037 min^{-1} and 0.033 min^{-1}, respectively). However, the lower K_I (0.037 μM vs 2 μM) of **26** suggests more

https://doi.org/10.1021/acs.jmedchem.6c01030
J. Med. Chem. XXXX, XXX, XXX−XXX

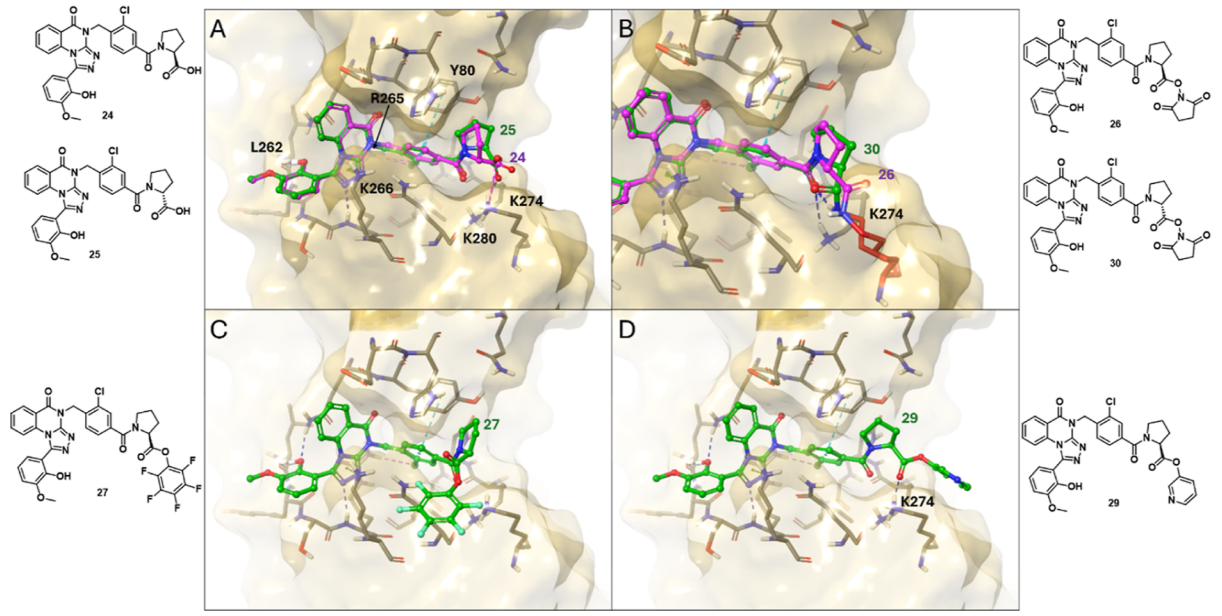

Figure 6. (A): Comparison of the predicted binding modes of compounds **24** (magenta) and **25** (green). (B): Experimental binding mode of compound **26** (PDB: 29CY, magenta) and predicted binding mode of **30** (green) resulted from covalent docking, zoomed into the covalent binding to residue K274 (colored in red). (C): Predicted binding mode of compound **27**. (D): Predicted binding mode of compound **29**. Interactions are shown as dashed lines, with light blue coloring corresponding to $\pi-\pi$ stacking, dark blue coloring corresponding to hydrogen bond, magenta coloring corresponding to salt bridges and purple coloring corresponding to halogen bonds.

Scheme 4. Synthesis of SHP244 and SHP844 Analogue Dichlorotriazines Having a Long (A) or a Short Linker (B)

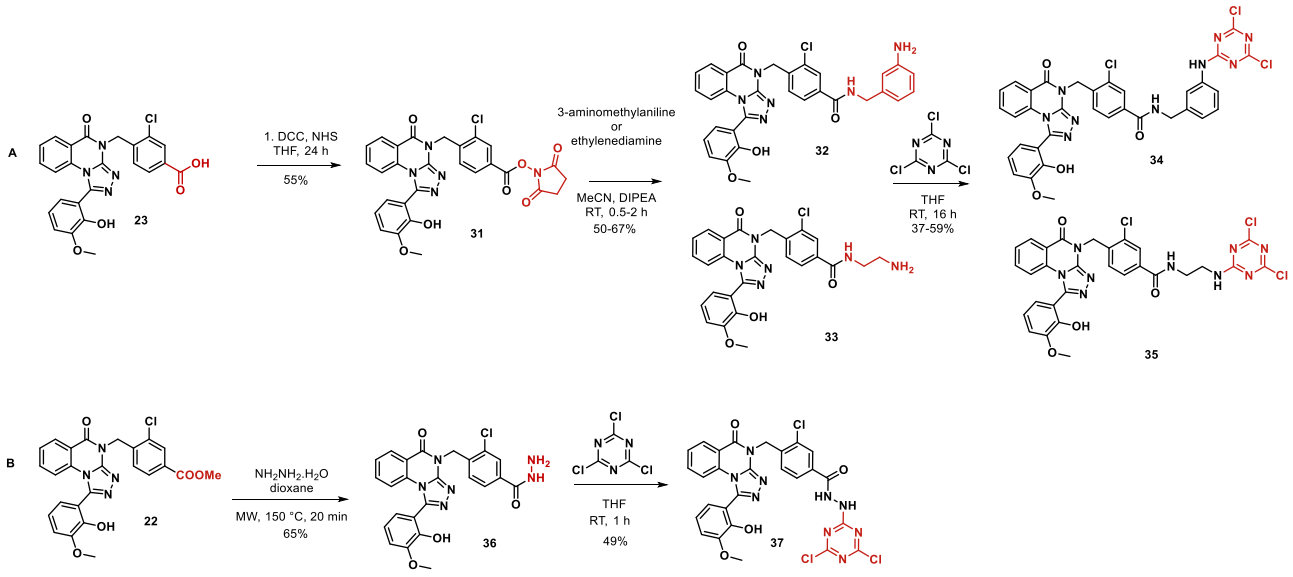

favorable non-covalent protein−ligand interactions contributing to the observed higher activity. We note that the k_{inact} values are close to the second generation EGFR-inhibitor dacomitinib (Vizimpro) used as a medication of non-small-cell lung carcinoma (NSCLC) (0.056 min^{-1}).[53,54]

Next, we investigated the inhibitory activity of compounds **SHP844** (**24**), **26** and **37** against SHP1 and PTP1B phosphatases in the fluorogenic DiFMUP assays (Figure S11). Based on available crystal structures, latch site seems almost conserved in SHP1 (PDB 2B30) and SHP2 (PDB 6BMR), however, in PTP1B (PDB 2CM2) the protein is more open at that surface, no real pocket can be identified (Figure S12). The reference compound **SHP844** showed modest (~3x) selectivity against these enzymes [IC_{50} ($SHP1^{FL}$) 75.3 μM, IC_{50} ($PTP1B^{FL}$) 62.5 μM] compared to SHP2 [IC_{50} ($SHP1^{FL}$) 18.9 μM]. The NHS ester **26** did not show any activity in 1 μM that suggest >60 fold preference for SHP2. The dichlorotriazine **37** provided 7−36 fold selectivity for SHP2 [IC_{50} ($SHP1^{FL}$) 3.6 μM, IC_{50} ($PTP1B^{FL}$) 18.1 μM]. These results support that covalent targeting at the latch side improves the selectivity for SHP2 over other related phosphatases.

Finally, we investigated whether **SHP844**, NHS-ester **26** and dichlorotriazine **37** could inhibit SHP2 in cells by measuring DUSP6 mRNA levels, a commonly used marker of the MAPK

https://doi.org/10.1021/acs.jmedchem.6c01030
J. Med. Chem. XXXX, XXX, XXX−XXX

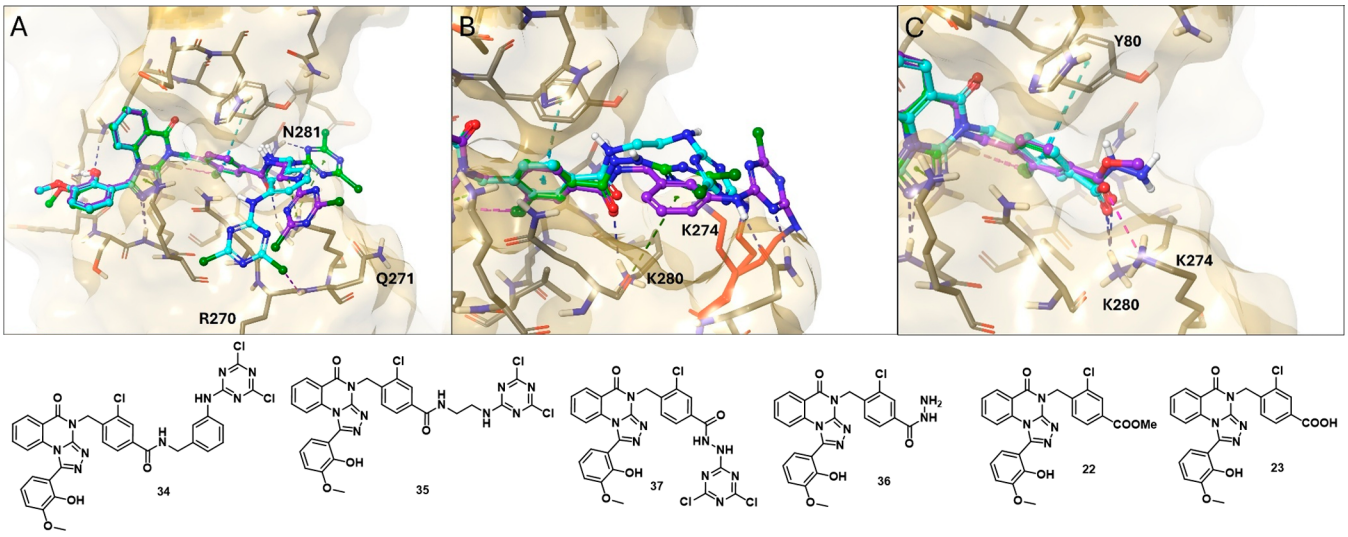

Figure 7. (A): Predicted binding modes of **34** (cyan coloring), **35** (purple coloring) and **37** (green coloring) resulted from non-covalent docking. (B): Predicted binding mode resulted from covalent docking for **34** (cyan coloring), **35** (purple coloring) and **37** (green coloring), with the K274 residue colored in red. (C): Predicted binding mode of hydrazide **36** (green coloring), carboxylic acid **23** (cyan coloring) and methyl ester **22** (purple coloring) zoomed into the terminal group. Interactions are shown as dashed lines, with light blue coloring corresponding to $\pi-\pi$ stacking, dark blue coloring corresponding to hydrogen bond, magenta coloring corresponding to salt bridges, green coloring corresponding to π-cation interactions and purple coloring corresponding to halogen bonds.

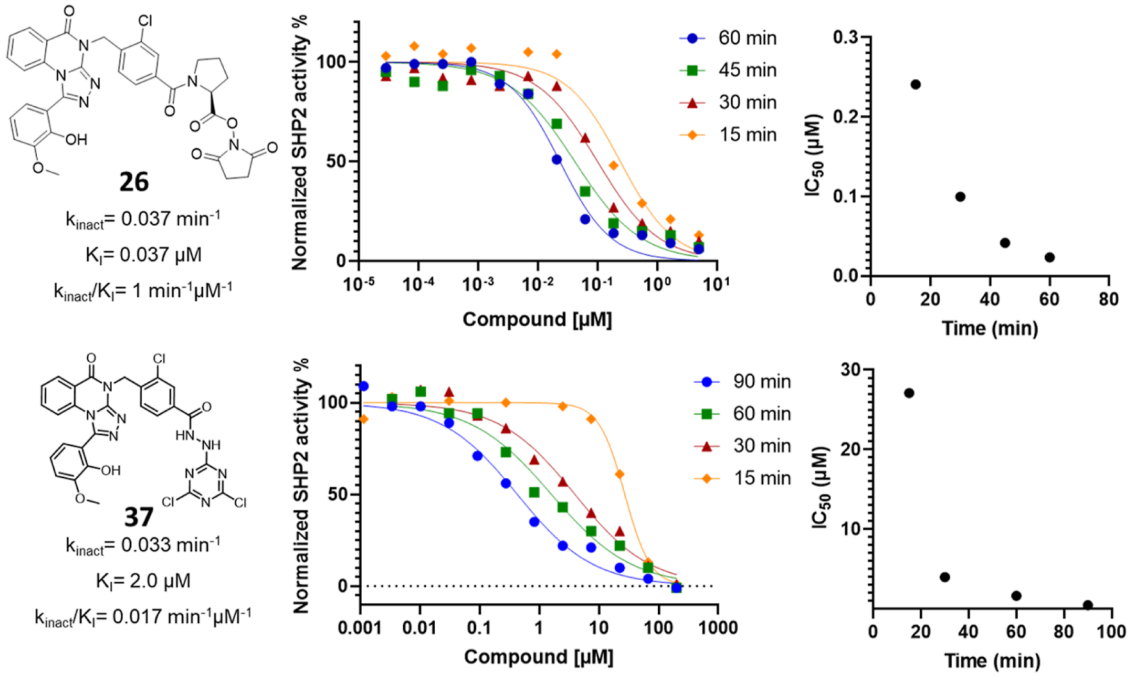

Figure 8. Time-dependent IC_{50} experiments with compounds **26** and **37**. The k_{inact} and K_I of the hit compounds were calculated by fitting endpoint pre-incubation IC_{50} data using the EPIC-Fit method.[52]

pathway downstream of SHP2. [36] The compounds were tested on human melanoma (A375, resistant on SHP2 inhibition) and human lung cancer (H1650, sensitive on SHP2 inhibition) cells in a single dose (1 μM). We found that cellular treatment did not affect the resistant A375 cell line, while there was a significant inhibition of the mRNA level of DUSP6 in H1650 cells for covalent inhibitors **37** (65.5%) and **26** (76.5%) (Figure 9). These data support the target engagement of the latch site covalent allosteric inhibitors, and present that these compounds exhibit activity against endogenous SHP2 also in its native environment in cells.

CONCLUSIONS

Here, we describe a proof-of-concept study for the identification, synthesis and biochemical characterization of lysine-targeting covalent allosteric inhibitors that engage lysine residues available at the latch site of SHP2. The study combines the electrophile-first warhead screening with a ligand-first covalent

https://doi.org/10.1021/acs.jmedchem.6c01030
J. Med. Chem. XXXX, XXX, XXX–XXX

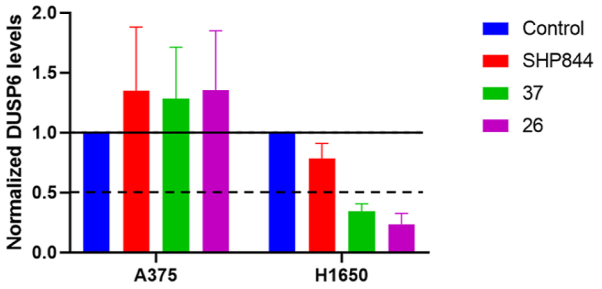

Figure 9. mRNA DUSP6 levels in 2 cancer cell lines after 2 h of the treatment with 1 μM concentration of SHP2 inhibitors **SHP844**, **26** and **37**. Relative gene expression was calculated using the $2^{-\Delta\Delta Cq}$ method where expressions were normalized to beta actin as a housekeeping gene and then expressions under treatments were normalized to the control for each cell line. Dashed line represents significant (more than 50%) downregulation.

strategy demonstrating that lysine covalent engagement can provide submicromolar and even nanomolar activities at the underexplored allosteric latch site of SHP2. In this context, NHS ester and dichlorotriazine warheads emerged as particularly effective chemotypes for lysine engagement of SHP2. Moreover, the developed inhibitors showed improved selectivity against SHP1 and PBP1B phosphatases and were proven to successfully target SHP2 in cellular environment. These results not only validate the latch site as a tractable allosteric locus for potent SHP2 modulation but establish lysine-directed covalent engagement as an effective approach for generating high-potency leads.

In addition, the reported SAR suggests several practical observations that might be useful for further covalent approaches targeting the latch site of SHP2. First, covalent activation (NHS ester or dichlorotriazine) can produce large improvements in potency relative to the corresponding non-activated acids or non-covalent precursors (e.g., (*S*)-**SHP844**-NHS, **26**, $IC_{50} = 15$ nM, $k_{inact}/K_I = 1$ min^{-1} μM^{-1}; **SHP244**-dichlorotriazine, **37**, $IC_{50} = 510$ nM, $k_{inact}/K_I = 0.017$ min^{-1} μM^{-1}). Second, we found that the proline moiety of the original ligands is not required to retain the activity in this series. This opens new options for E-ring optimization with reduced synthetic complexity and faster analogue synthesis. Third, specific stereocenters introduced by the proline moiety and substituents of the D (e.g. *ortho*-OH) and the E ring (e.g. *ortho* halogen) appear to influence activity and will be important handles in future optimization campaigns. Finally, driven by our covalent approach we identified non-covalent inhibitors that outperform previously reported ligands for the latch site (IC_{50}s > 18 μM).[36−39] Thus, covalent approaches deliver not only high-potency covalent compounds but also reveal the underlying non-covalent interaction network useful to design new, reversible high-affinity ligands.

EXPERIMENTAL SECTION

This research did not involve human or animal participants.

General Chemistry Methods

Reagents and solvents were obtained from commercial sources (Sigma-Aldrich, Fluorochem, Enamine, BLDPharma and Ambeed). Reactions were monitored using analytical thin-layer chromatography plates (Merck 60 F254, 0.20 mm), and the components were visualized under UV light and/or through staining with the relevant reagent. Flash column chromatography was performed using a CombiFlash Rf 200 device (Teledyne ISCO, Lincoln, NE, USA), and in the case of reversed phase chromatography RediSep Rf reversed phase C18 columns were used. Normal phase flash column chromatography was performed on Merck Silica Gel 60 (particle size 0.040−0.063 mm). Melting points were determined on a Reichelt hot-stage apparatus, and are uncorrected. ^{1}H and ^{13}C NMR spectra were recorded at 295 K on a Varian System 500 NMR spectrometer (Varian, Palo Alto, CA, USA) or a Varian System 300 NMR spectrometer operating at frequencies for ^{1}H NMR at 600 MHz, 500 MHz or 300 MHz, and for ^{13}C NMR at 150 MHz, 125 MHz or 75 MHz, respectively. The chemical shifts (δ) are reported in parts per million (ppm) and are referenced to the deuterated solvent used. The coupling constants (J) are given in Hz, and the splitting patterns are designated as follows: s, singlet; br s, broad singlet; d, doublet; app d, apparent doublet; dd, double doublet; ddd, doublet of doublets of doublets; t, triplet; dt, doublet of triplets; td, triplet of doublets; m, multiplet. All ^{13}C NMR spectra were proton decoupled. HPLC-MS measurements were performed using a Shimadzu LC-MS-2020 device (Shimadzu Corporation, Kyoto, Japan) equipped with a Reprospher 100 C18 (5 μm, 100 × 3 mm) column and positive-negative double ion source (DUIS±) with a quadrupole mass spectrometer in a range of 50−1000 m/z. The sample was eluted with gradient elution using eluent A (0.1% HCOOH in H_2O) and eluent B (0.1% HCOOH in MeCN). The flow rate was set to 1.5 mL/min. The initial condition was 0% B eluent, followed by a linear gradient to 100% B eluent by 2 min, from 2 to 3.75 min 100% B eluent was retained, and from 3.75 to 4.5 min back to the initial condition and retained to 5 min. The column temperature was kept at 30 °C and the injection volume was 1 μL. The synthesis of the compounds **3**−**5** followed the methods described in the literature without modification.[36] All compounds are >95% pure by HPLC analysis.

Synthetic Procedures and Characterization of the Compounds

3-((*E*)-(((*E*)-3-(2-Chlorobenzyl)-4-oxo-3,4-dihydroquinazolin-2(1*H*)-ylidene)hydrazineylidene)methyl)benzoic acid (8). A solution of hydrazone (**5**, 180 mg, 0.60 mmol, 1.0 eq.) and 3-formylbenzoic acid (90 mg, 0.60 mmol, 1 eq.) was dissolved in isopropanol (5 mL), followed by the addition of acetic acid (1.8 μL, 0.032 mmol, 0.05 eq.). The reaction mixture was heated to 100 °C and stirred for 1 h. Upon cooling on ice, a precipitate formed, which was collected by filtration, washed with isopropanol (2 × 5 mL), and dried. The crude product was used directly in the next step without further purification. Yield: 0.179 g (69%), yellow crystals, mp 265 °C (isopropanol). ^{1}H NMR (300 MHz, DMSO-d_6): δ 10.77 (s, 1H), 8.37 (d, J = 9.3 Hz, 2H), 8.27 (d, J = 7.9 Hz, 1H), 8.03−7.86 (m, 2H), 7.76−7.65 (m, 2H), 7.60−7.46 (m, 2H), 7.32−7.15 (m, 3H), 7.13−7.03 (m, 1H), 5.37 (s, 2H). ^{13}C NMR (75 MHz, $CDCl_3$): δ 167.3, 160.4, 152.9, 150.0, 139.7, 135.5, 135.1, 134.1, 131.6, 130.3, 129.2, 128.9, 128.6, 128.3, 127.3, 126.5, 122.1, 115.9, 113.5, 42.1. HRMS (ESI$^+$) m/z: [M + H]$^+$, calcd for $C_{23}H_{18}N_4O_3Cl$, 433.1067; found, 433.1068. Purity by HPLC: 100%.

4-((*E*)-(((*E*)-3-(2-Chlorobenzyl)-4-oxo-3,4-dihydroquinazolin-2(1*H*)-ylidene)hydrazineylidene)-methyl)benzoic acid (9). Hydrazone derivative **5** (500 mg, 1.67 mmol, 1.0 eq.) and 4-formylbenzoic acid (250 mg, 1.67 mmol, 1.0 eq.) were dissolved in isopropanol (15 mL). Acetic acid (5 μL, 0.088 mmol, 0.05 eq.) was added, and the reaction mixture was stirred in a sealed tube at 100 °C for 1 h. Upon cooling, a yellow precipitate formed, which was collected by filtration, washed with isopropanol (2 × 10 mL), and dried in air. The crude product was used in the next step without further purification. Yield: 0.542 g (75%), white crystals, mp 267 °C (isopropanol). ^{1}H NMR (300 MHz, DMSO-d_6): δ 10.75 (s, 1H), 8.33 (s, 1H), 8.07 (d, J = 8.2 Hz, 2H), 8.01−7.90 (m, 3H), 7.72 (d, J = 4.1 Hz, 2H), 7.49 (dd, J = 7.5, 1.8 Hz, 1H), 7.24 (dtd, J = 16.2, 8.2, 5.2 Hz, 3H), 7.12−7.02 (m, 1H), 5.36 (s, 2H). ^{13}C NMR (75 MHz, DMSO-d_6): δ 204.7, 198.0, 190.1, 188.1, 177.3, 176.8, 172.8, 171.7, 169.2, 169.0, 167.0, 166.9, 166.0, 165.4, 165.0, 164.2, 159.9, 151.3. HRMS (ESI$^+$) m/z [M + H]$^+$, calcd for $C_{23}H_{18}N_4O_3Cl$, 433.1067; found, 433.1062. Purity by HPLC: 100%.

https://doi.org/10.1021/acs.jmedchem.6c01030
J. Med. Chem. XXXX, XXX, XXX−XXX

3-(4-(2-Chlorobenzyl)-5-oxo-4,5-dihydro-[1,2,4]triazolo[4,3-*a*]quinazolin-1-yl)benzoic Acid (10). Compound **8** (178 mg, 0.41 mmol, 1 eq.) was dissolved in ethanol (10 mL), and 2 M $FeCl_3$ solution (0.656 mmol, 0.33 mL, 1.6 eq.) was added. The resulting mixture was stirred at 80 °C for 3 h. Upon completion, the reaction mixture was purified by reverse-phase flash chromatography using water and acetonitrile as eluents to afford the desired product (**10**). Yield: 0.109 g (62%), orange crystals. ^{1}H NMR (300 MHz, DMSO-d_6): δ 8.37−8.16 (m, 3H), 8.06−7.48 (m, 5H), 7.42−6.99 (m, 4H), 5.49 (s, 2H). ^{13}C NMR (75 MHz, DMSO-d_6): δ 166.6, 158.4, 148.7, 147.4, 134.7, 134.0, 133.8, 132.8, 131.9, 131.7, 131.4, 130.6, 129.7, 129.3, 129.3, 128.9, 128.9, 127.4, 127.3, 126.8, 117.3, 115.7, 43.8. HRMS (ESI$^+$) m/z: $[M + H]^+$, calcd for $C_{23}H_{16}N_4O_3Cl$, 431.0910; found, 431.0910. Purity by HPLC: 100%.

4-(4-(2-Chlorobenzyl)-5-oxo-4,5-dihydro-[1,2,4]triazolo[4,3-*a*]quinazolin-1-yl)benzoic Acid (11). Compound **9** (349 mg, 0.81 mmol, 1.0 eq.) was dissolved in ethanol (15 mL), and 2 M $FeCl_3$ solution (0.64 mL, 1.30 mmol, 1.6 eq.) was added. The reaction mixture was heated to 80 °C and stirred for 3 h. After completion, the ethanol was evaporated, and the crude product was purified by reverse-phase flash chromatography using water and acetonitrile as eluents. Yield: 0.223 g (64%), white powder. ^{1}H NMR (300 MHz, DMSO-d_6): δ 8.28 (d, J = 7.8 Hz, 1H), 8.20 (d, J = 7.9 Hz, 2H), 7.86 (d, J = 7.9 Hz, 2H), 7.71 (t, J = 7.5 Hz, 1H), 7.56 (dd, J = 10.5, 7.7 Hz, 2H), 7.38−7.22 (m, 3H), 7.14 (d, J = 8.4 Hz, 1H), 5.49 (s, 2H). ^{13}C NMR (75 MHz, DMSO-d_6): δ 166.8, 158.4, 148.8, 147.5, 134.8, 133.9, 132.9, 132.8, 132.4, 131.7, 130.0, 129.3, 129.0, 127.4, 127.3, 126.8, 117.3, 115.8, 43.9. HRMS (ESI$^+$) m/z: $[M + H]^+$ calcd for $C_{23}H_{16}N_4O_3Cl$, 431.0910; found, 431.0908. Purity by HPLC: 100%.

2,5-Dioxopyrrolidin-1-yl 3-(4-(2-chlorobenzyl)-5-oxo-4,5-dihydro-[1,2,4]triazolo[4,3-*a*]quinazolin-1-yl)benzoate (12). Compound **10** (30 mg, 0.07 mmol, 1.0 eq.) was dissolved in anhydrous THF (2 mL), followed by the sequential addition of *N*,*N*′-dicyclohexylcarbodiimide (13 μL, 0.084 mmol, 1.2 eq.) and *N*-hydroxysuccinimide (9.7 mg, 0.084 mmol, 1.2 eq.). The reaction mixture was stirred at room temperature for 24 h. The crude mixture was purified by reverse-phase flash chromatography using water and acetonitrile as eluents to afford the corresponding NHS ester (**12**). Yield: 0.022 g (60%), white crystals. ^{1}H NMR (300 MHz, $CDCl_3$): δ 8.50−8.35 (m, 3H), 8.01 (d, J = 7.8 Hz, 1H), 7.78 (d, J = 7.7 Hz, 1H), 7.62−7.47 (m, 2H), 7.41 (d, J = 7.7 Hz, 1H), 7.24−7.12 (m, 4H), 5.73 (s, 2H), 2.90 (s, 4H). ^{13}C NMR (75 MHz, $CDCl_3$): δ 169.1, 161.1, 158.5, 147.3, 136.1, 135.0, 133.4, 132.9, 132.7, 131.9, 130.9, 130.1, 129.9, 129.6, 129.0, 127.8, 127.5, 127.1, 126.6, 117.7, 115.8, 44.7, 25.8. HRMS (ESI$^+$) m/z: $[M + H]^+$, calcd for $C_{27}H_{19}N_5O_5Cl$, 528.1074; found, 528.1068. Purity by HPLC: 100%.

2,5-Dioxopyrrolidin-1-yl 4-(4-(2-chlorobenzyl)-5-oxo-4,5-dihydro-[1,2,4]triazolo[4,3-*a*]quinazolin-1-yl)benzoate (13). A solution of compound **11** (57 mg, 0.13 mmol, 1.0 eq.), *N*,*N*′-dicyclohexylcarbodiimide (25 μL, 0.16 mmol, 1.2 eq.), and *N*-hydroxysuccinimide (18 mg, 0.16 mmol, 1.2 eq.) was dissolved in anhydrous THF (2 mL). The reaction mixture was stirred at room temperature for 24 h. Upon completion, the crude mixture was purified by reverse-phase flash chromatography using water and acetonitrile as eluents to afford the desired product (**13**). Yield: 0.025 g (36%), white crystals. ^{1}H NMR (300 MHz, DMSO-d_6): δ 8.37 (d, J = 6.8 Hz, 1H), 8.30 (d, J = 7.9 Hz, 0H), 8.03 (dd, J = 8.2, 1.4 Hz, 1H), 7.77 (t, J = 1.7 Hz, 0H), 7.63−7.49 (m, 1H), 7.40−7.18 (m, 2H), 5.51 (s, 1H), 2.94 (s, 2H). ^{13}C NMR (75 MHz, DMSO-d_6): δ 170.3, 161.4, 158.4, 149.1, 147.0, 135.0, 134.9, 133.8, 132.8, 131.7, 130.8, 129.3, 129.0, 127.4, 127.3, 126.9, 126.3, 117.3, 116.2, 54.9, 43.9, 25.6. HRMS (ESI$^+$) m/z: $[M + H]^+$, calcd for $C_{27}H_{19}N_5O_5Cl$, 528.1074; found, 528.1062. Purity by HPLC: 100%.

3-(4-Methoxybenzyl)-2-thioxo-2,3-dihydroquinazolin-4(1*H*)-one (15). A solution of 2-methoxycarbonylphenyl isothiocyanate (**14**, 10.4 g, 54.0 mmol, 1.0 eq.) and 4-methoxybenzylamine (14.1 mL, 108 mmol, 2.0 eq.) in toluene (75 mL) was stirred at room temperature for 1 h in the presence of DIPEA (18.8 mL, 108.0 mmol, 2.0 eq.). Upon completion of the reaction, the precipitated solid was collected by filtration, washed twice with toluene (2 × 10 mL), and dried under reduced pressure. The crude product was used directly in the next step without further purification. Yield: 15.8 g (98%), white crystals, mp 228 °C (toluene). ^{1}H NMR (300 MHz, DMSO-d_6): δ 12.98 (br, 1H), 7.94 (dd, J = 8.0, 1.5 Hz, 1H), 7.73 (ddd, J = 8.5, 7.2, 1.5 Hz, 1H), 7.40 (d, J = 8.2 Hz, 1H), 7.37−7.28 (m, 3H), 6.84 (d, J = 8.6 Hz, 1H), 5.59 (s, 2H), 3.70 (s, 3H). ^{13}C NMR (75 MHz, DMSO-d_6): δ 175.5, 159.4, 158.4, 139.1, 135.6, 129.0, 128.6, 127.3, 124.6, 115.7, 115.5, 113.6, 55.0, 48.1. HRMS (ESI$^+$) m/z: $[M + H]^+$, calcd for $C_{16}H_{15}N_2O_2S$: 299.0854; found, 299.0854. Purity by HPLC: 100%.

(*E*)-2-Hydrazineylidene-3-(4-methoxybenzyl)-2,3-dihydroquinazolin-4(1*H*)-one (16). Dihydroquinazoline derivative (**15**, 15.2 g, 51.0 mmol, 1.0 eq.) was dissolved in isopropanol (300 mL), after which hydrazine monohydrate (62% aqueous solution of hydrazine, 26.6 mL, 510.0 mmol, 10.0 eq.) was added. The resulting mixture was stirred at 90 °C for 24 h. Upon cooling to room temperature, a yellow precipitate formed. The solid was collected by filtration, washed with water (3 × 15 mL), and dried under reduced pressure. The crude product was used directly in the next synthetic step without further purification. Yield: 14.1 g (93%), yellow crystals, mp 177 °C (water). ^{1}H NMR (300 MHz, DMSO-d_6): δ 7.94 (dd, J = 7.9, 1.6 Hz, 1H), 7.60 (ddd, J = 8.5, 7.1, 1.7 Hz, 1H), 7.32 (dt, J = 8.2, 1.0 Hz, 1H), 7.21 (d, J = 8.7 Hz, 2H), 7.13 (t, J = 7.4 Hz, 1H), 6.85 (d, J = 8.7 Hz, 2H), 5.18 (s, 2H), 3.70 (s, 3H). ^{13}C NMR (75 MHz, DMSO-d_6): δ 161.5, 158.4, 134.4, 128.6, 128.5, 126.9, 121.8, 113.7, 55.1, 42.1. HRMS (ESI$^+$) m/z: $[M + H]^+$, calcd for $C_{16}H_{17}N_4O_2$, 297.1351; found, 297.1343. Purity by HPLC: 100%.

(*E*)-2-(((*E*)-2-Hydroxy-3-methoxybenzylidene)hydrazineylidene)-3-(4-methoxybenzyl)-2,3-dihydro-quinazolin-4(1*H*)-one (17). Hydrazone derivative (**16**, 7.0 g, 23.6 mmol, 1.0 eq.) and *o*-vanillin (3.6 g, 23.6 mmol, 1.0 eq.) were dissolved in isopropanol (50 mL), followed by the addition of acetic acid (38.5 μL, 0.67 mmol, 0.03 eq.). The mixture was stirred at 100 °C for 1 h in a sealed tube. After completion, the reaction mixture was cooled in an ice-water bath, resulting in the formation of a yellow precipitate. The solid was collected by filtration, dried in air, and used in the subsequent step without further purification. Yield: 9.1 g (90%), yellow crystals, mp 126 °C (isopropanol). ^{1}H NMR (300 MHz, DMSO-d_6): δ 10.59 (s, 1H), 9.83 (s, 1H), 8.63 (s, 1H), 7.93 (dd, J = 7.9, 1.5 Hz, 1H), 7.67−7.49 (m, 3H), 7.43−7.36 (m, 2H), 7.15 (ddd, J = 8.0, 6.8, 1.4 Hz, 1H), 7.01 (dd, J = 8.0, 1.5 Hz, 1H), 6.87 (d, J = 8.4 Hz, 3H), 5.23 (s, 2H), 3.83 (s, 3H), 3.70 (s, 3H). ^{13}C NMR (75 MHz, DMSO-d_6): δ 160.3, 158.3, 152.8, 148.7, 147.9, 146.4, 139.5, 134.9, 129.5, 129.4, 127.3, 122.0, 120.7, 120.6, 118.9, 115.7, 113.6, 113.6, 113.3, 55.9, 55.0, 43.0. HRMS (ESI$^+$) m/z: $[M + H]^+$, calcd for $C_{24}H_{23}N_4O_4$, 431.1719; found, 431.1713. Purity by HPLC: 100%.

1-(2-Hydroxy-3-methoxyphenyl)-4-(4-methoxybenzyl)-[1,2,4]triazolo[4,3-*a*]quinazolin-5(4*H*)-one (18). Dihydroquinazoline derivative (**17**, 8.90 g, 20.7 mmol, 1.0 eq.) was dissolved in ethanol (400 mL), followed by the addition of aqueous $FeCl_3$ solution (2 M, 16.6 mL, 33.1 mmol, 1.6 eq.). The reaction mixture was stirred at 80 °C for 4 h. After cooling with an ice-water bath, the resulting precipitate was collected by filtration and washed with ethanol (2 × 10 mL). The crude product was used directly in the subsequent step without further purification. Yield: 7.97 g (89%), yellow crystals, mp 198 °C (ethanol). ^{1}H NMR (300 MHz, DMSO-d_6): δ 9.45 (s, 1H), 8.26 (dd, J = 7.9, 1.6 Hz, 1H), 7.68 (ddd, J = 8.6, 7.4, 1.7 Hz, 1H), 7.56−7.44 (m, 3H), 7.27 (dd, J = 7.6, 2.1 Hz, 1H), 7.16−7.11 (m, 1H), 7.08−6.98 (m, 2H), 6.90 (d, J = 8.7 Hz, 2H), 5.37 (s, 2H), 3.89 (s, 3H), 3.72 (s, 3H). ^{13}C NMR (75 MHz, DMSO-d_6): δ 159.3, 158.5, 148.6, 148.4, 146.2, 145.9, 135.3, 134.1, 130.4, 129.5, 128.6, 127.1, 123.2, 120.2, 117.2, 116.7, 115.6, 115.0, 114.3, 56.5, 55.5, 45.7. HRMS (ESI$^+$) m/z: $[M + H]^+$, calcd for $C_{24}H_{21}N_4O_4$, 429.1562; found, 429.1557. Purity by HPLC: 100%.

1-(3-Methoxy-2-((triisopropylsilyl)oxy)phenyl)-4-(4-methoxybenzyl)-[1,2,4]triazolo[4,3-*a*]quinazolin-5(4*H*)-one (19). Quinazoline derivative (**18**, 5.78 g, 13.5 mmol, 1.0 eq.) was dissolved in DIPEA (28 mL) under nitrogen atmosphere. Triisopropylsilyl chloride (17.3 mL, 81.0 mmol, 6.0 eq.) was added dropwise at room temperature. The reaction mixture was stirred at 40 °C for 2 h. Upon completion, the mixture was concentrated under reduced pressure to a volume of 5 mL. The resulting brown oil was dissolved in dichloromethane (30 mL) and filtered through a short pad of celite. The filtrate was concentrated and the crude product was purified by normal-phase flash chromatography (hexanes/EtOAc gradient) to

https://doi.org/10.1021/acs.jmedchem.6c01030
J. Med. Chem. XXXX, XXX, XXX−XXX

afford the silylated product (**19**) as a colorless oil. Yield: 4.42 g (56%), yellow crystals, mp 151 °C (hexanes/EtOAc). ^{1}H NMR (300 MHz, DMSO-d_6): δ 8.25 (dd, J = 7.9, 1.6 Hz, 1H), 7.65 (t, J = 7.5 Hz, 1H), 7.57−7.43 (m, 3H), 7.35 (dd, J = 7.7, 2.2 Hz, 1H), 7.19−7.04 (m, 3H), 6.89 (d, J = 8.3 Hz, 2H), 5.46−5.30 (m, 2H), 3.86 (s, 3H), 3.71 (s, 3H), 0.83 (h, J = 7.4 Hz, 3H), 0.62−0.53 (m, 18H). ^{13}C NMR (75 MHz, DMSO-d_6): δ 159.3, 158.3, 150.0, 148.6, 145.9, 144.6, 135.2, 134.0, 130.5, 129.4, 128.6, 127.3, 123.2, 122.2, 120.7, 117.2, 115.5, 115.2, 114.2, 55.8, 55.6, 45.5, 17.8, 17.7, 13.6. HRMS (ESI$^+$) m/z: [M + H]$^+$ calcd for $C_{33}H_{41}N_4O_4Si$, 585.2897; found, 585.2875. Purity by HPLC >98%.

1-(3-Methoxy-2-((triisopropylsilyl)oxy)phenyl)-[1,2,4]triazolo[4,3-*a*]quinazolin-5(4*H*)-one (20). Quinazoline derivative (**19**, 3.5 g, 6.0 mmol, 1.0 eq.) was dissolved in anhydrous dichloromethane (150 mL) under nitrogen atmosphere. Trifluoromethanesulfonic acid (2.65 mL, 30.0 mmol, 5.0 eq.) was added dropwise at room temperature and the reaction mixture was stirred at ambient temperature for 16 h. Reaction progress was monitored by HPLC-MS, which confirmed the formation of the desired product (**20**). Concurrently, a side product, identified as the non-triflated analogue of **20** was detected. To minimize side-product formation, the reaction was quenched at approximately 90% conversion by the sequential addition of 5% aqueous sodium bicarbonate solution (15 mL) and 20 mL of methanol under stirring. The resulting white precipitate was collected by filtration and washed with cold dichloromethane (3 × 20 mL). The aqueous phase was extracted with dichloromethane (3 × 50 mL), and the combined organic layers were dried over anhydrous $MgSO_4$. The solvent was removed under reduced pressure and the crude product was purified by reversed-phase flash chromatography using a gradient of water and acetonitrile as eluents. Yield: 1.37 g (49%), white crystals, mp 70 °C (water/acetonitrile). ^{1}H NMR (300 MHz, $CDCl_3$): δ 9.09 (br, 1H), 8.39 (dd, J = 7.7, 1.8 Hz, 1H), 7.54−7.36 (m, 2H), 7.27−7.22 (m, 1H), 7.18 (dd, J = 7.1, 2.1 Hz, 1H), 7.14−7.02 (m, 2H), 3.86 (s, 3H), 0.92 (h, J = 7.4 Hz, 3H), 0.71 (dd, J = 7.4, 3.3 Hz, 18H). ^{13}C NMR (75 MHz, $CDCl_3$): δ 159.8, 149.9, 148.0, 145.3, 145.1, 134.7, 129.6, 126.8, 123.5, 121.6, 120.4, 117.7, 116.1, 114.1, 55.0, 17.7, 17.6, 13.8. HRMS (ESI$^+$) m/z: [M + H]$^+$, calcd for $C_{25}H_{33}N_4O_3Si$, 465.2321; found, 466.2321. Purity by HPLC >98%.

3-Chloro-4-((1-(2-hydroxy-3-methoxyphenyl)-5-oxo-[1,2,4]triazolo[4,3-*a*]quinazolin-4(5*H*)-yl)methyl)benzonitrile (21). Compound **20** (1.11 g, 2.39 mmol, 1.0 eq.) was dissolved in DMF (10 mL) under argon atmosphere. Lithium bis(trimethylsilyl)amide (0.535 mL, 2.75 mmol, 1.15 eq., 2 M THF solution) was added dropwise to the reaction mixture, which was then stirred at room temperature for 15 min. After that, 4-(bromomethyl)-3-chlorobenzonitrile (0.4378 mL, 0.678 g, 2.94 mmol, 1.2 eq.) was added, and the mixture was stirred at room temperature for an additional 2 h. To remove the TIPS protecting group, KHF_2 (0.933 g, 11.9 mmol, 5.0 eq.) and trifluoroacetic acid (0.549 mL, 7.17 mmol, 3.0 eq.) were sequentially added to the reaction mixture. Stirring was continued for 1 h at room temperature. Then, the reaction mixture was concentrated under reduced pressure and the crude product was purified directly by reversed-phase flash chromatography using water and acetonitrile as eluents. Yield: 0.752 g (69%), white crystals, mp 187 °C (water/acetonitrile). ^{1}H NMR (300 MHz, CD_3OD): δ 8.37−8.32 (m, 1H), 7.94 (d, J = 1.6 Hz, 1H), 7.71 (dd, J = 8.1, 1.6 Hz, 1H), 7.64−7.55 (m, 3H), 7.35−7.28 (m, 2H), 7.19−7.04 (m, 2H), 5.69 (s, 2H), 3.99 (s, 3H). HRMS (ESI$^+$) m/z: [M + H]$^+$, calcd for $C_{24}H_{17}N_5O_3Cl$, 458.1019; found, 458.1019. Purity by HPLC >98%.

Methyl 3-Chloro-4-((1-(2-hydroxy-3-methoxyphenyl)-5-oxo-[1,2,4]triazolo[4,3-*a*]quinazolin-4(5*H*)-yl)methyl)benzoate (22). Compound **20** (1.11 g, 2.39 mmol, 1.0 eq.) was dissolved in DMF (10 mL). Potassium bis(trimethylsilyl)amide (0.548 g, 2.75 mmol, 1.15 eq.) was added to the reaction mixture, subsequently stirred at room temperature for 10 min. Then, methyl 4-(bromomethyl)-3-chlorobenzoate (0.631 g, 2.39 mmol, 1.0 eq.) was added, and the mixture was stirred at ambient temperature for 1 h. TIPS protecting group was also removed under these conditions. The reaction mixture was concentrated under reduced pressure, and the crude product was purified directly by reversed-phase flash chromatography using water + 0.1% HCOOH and acetonitrile + 0.1% HCOOH as eluents. Yield: 0.645 g (55%), brown-grey solid. ^{1}H NMR (500 MHz, CD_3OD): δ 8.39 (dd, J = 7.9, 1.6 Hz, 1H), 8.12 (d, J = 1.7 Hz, 1H), 7.88 (dd, J = 8.1, 1.7 Hz, 1H), 7.68 (ddd, J = 8.7, 7.4, 1.6 Hz, 1H), 7.62−7.54 (m, 1H), 7.38 (d, J = 8.4 Hz, 1H), 7.34−7.28 (m, 2H), 7.19−7.06 (m, 2H), 5.70 (d, J = 7.7 Hz, 2H), 3.99 (s, 3H), 3.92 (s, 3H). ^{13}C NMR (126 MHz, DMSO-d_6): δ 157.50, 150.92, 140.73, 140.12, 130.00, 126.65, 126.18, 124.71, 122.70, 121.98, 121.03, 119 HRMS (ESI$^+$) m/z: [M + H]$^+$, calcd for $C_{25}H_{20}N_4O_5Cl$, 491.11; found, 491.1116. Purity by HPLC: 100%.

3-Chloro-4-((1-(2-hydroxy-3-methoxyphenyl)-5-oxo-[1,2,4]triazolo[4,3-*a*]quinazolin-4(5*H*)-yl)methyl)benzoic acid (23). Benzonitrile (**21**, 0.284 g, 0.620 mmol) was dissolved in a mixture of 1,4-dioxane (20 mL), and concentrated hydrochloric acid (10 mL, 36−38% w/w). The reaction mixture was stirred at 80 °C for 24 h. Upon completion, the reaction mixture was concentrated under reduced pressure. The crude residue was subjected to reversed-phase flash using water and acetonitrile as eluents to afford the corresponding carboxylic acid derivative (**23**). Yield: 210 mg (70%), white crystals, mp 180 °C (water/acetonitrile). ^{1}H NMR (300 MHz, DMSO-d_6): δ 9.52 (s, 1H), 8.27 (d, J = 7.8 Hz, 1H), 8.00 (d, J = 1.6 Hz, 1H), 7.82−7.70 (m, 2H), 7.57 (t, J = 7.7 Hz, 1H), 7.38 (d, J = 8.1 Hz, 1H), 7.29 (dd, J = 6.9, 2.8 Hz, 1H), 7.20 (d, J = 8.4 Hz, 1H), 7.07−7.00 (m, 2H), 5.53 (s, 2H), 3.90 (s, 3H). ^{13}C NMR (75 MHz, DMSO-d_6): δ 166.0, 158.5, 148.3, 148.0, 145.8, 138.0, 135.1, 134.1, 132.0, 131.7, 129.9, 129.2, 128.2, 127.8, 126.9, 122.8, 119.9, 116.9, 116.1, 115.3, 114.7, 56.2, 44.2. HRMS (ESI$^+$) m/z: [M + H]$^+$, calcd for $C_{24}H_{18}N_4O_5Cl$, 477.0965; found, 477.0965. Purity by HPLC: 100%.

Alternative Synthesis of 23 from Methyl 3-Chloro-4-((1-(2-hydroxy-3-methoxyphenyl)-5-oxo-[1,2,4]triazolo[4,3-*a*]quinazolin-4(5*H*)-yl)methyl)benzoate (22). Methyl 3-chloro-4-((1-(2-hydroxy-3-methoxyphenyl)-5-oxo-[1,2,4]triazolo[4,3-*a*]quinazolin-4(5H)-yl)methyl)benzoate (**22**, 207 mg, 0.42 mmol, 1 eq.) and KCN (55.0 mg, 0.84 mmol, 2 eq.) dissolved in a mixture of 1,4-dioxane/H_2O (2:1, 2.4 mL) and left stirring at 100 °C for 4 h. The solvent was evaporated and the product was purified by reverse-phase flash chromatography using H_2O + 0.1% HCOOH and MeCN + 0.1% HCOOH as eluents. Yield: 0.104 g (52%), white crystals.

(3-Chloro-4-((1-(2-hydroxy-3-methoxyphenyl)-5-oxo-[1,2,4]triazolo[4,3-*a*]quinazolin-4(5*H*)-yl)methyl)benzoyl)-L-proline (24). NHS ester derivative **31** (86 mg, 0.15 mmol, 1.0 eq.) and L-proline (17 mg, 0.15 mmol, 1.0 eq.) were dissolved in dimethyl sulfoxide (0.6 mL). The reaction mixture was stirred at room temperature for 1 h. The crude reaction mixture was purified directly by preparative reversed-phase HPLC using water and acetonitrile as eluents. Yield: 0.056 g (55%), white crystals, mp 212 °C (water/acetonitrile). ^{1}H NMR (300 MHz, CD_3OD): δ 8.25 (dd, J = 7.7, 1.9 Hz, 1H), 8.05 (s, 1H), 7.66−7.54 (m, 2H), 7.53−7.43 (m, 2H), 7.32 (dd, J = 18.6, 8.3 Hz, 1H), 7.23 (dd, J = 7.9, 1.8 Hz, 2H), 7.10−6.95 (m, 2H), 5.59 (s, 2H), 4.51 (dd, J = 8.5, 5.2 Hz, 1H), 3.91 (s, 3H), 3.70−3.42 (m, 2H), 2.41−2.23 (m, 1H), 2.07−1.79 (m, 3H). HRMS (ESI$^+$) m/z: [M + H]$^+$, calcd for $C_{29}H_{25}N_5O_6Cl$, 574.1493; found, 574.1484. Purity by HPLC: 100%.

(3-Chloro-4-((1-(2-hydroxy-3-methoxyphenyl)-5-oxo-[1,2,4]triazolo[4,3-*a*]quinazolin-4(5*H*)-yl)methyl)benzoyl)-D-proline (25). NHS ester derivative **31** (86 mg, 0.15 mmol, 1.0 eq.) and D-proline (17 mg, 0.15 mmol, 1.0 eq.) were dissolved in dimethyl sulfoxide (1.2 mL). The reaction mixture was stirred at room temperature for 1 h. The crude reaction mixture was purified directly by preparative reversed-phase HPLC using water and acetonitrile as eluents. Yield: 0.064 g (74%), white crystals, mp 210 °C (water/acetonitrile). ^{1}H NMR (500 MHz, DMSO-d_6): δ 8.32−8.19 (m, 1H), 7.76−7.47 (m, 3H), 7.41−7.27 (m, 2H), 7.27−7.14 (m, 1H), 7.15−6.99 (m, 2H), 5.50 (d, J = 21.0 Hz, 2H), 4.37 (dd, J = 7.6, 4.5 Hz, 1H), 4.09 (d, J = 5.6 Hz, 1H), 3.89 (d, J = 9.9 Hz, 3H), 3.52−3.42 (m, 2H), 2.07−1.74 (m, 3H). HRMS (ESI$^+$) m/z: [M + H]$^+$, calcd for $C_{29}H_{25}ClN_5O_6$, 574.1487; found, 574.1512. Purity by HPLC: 100%.

https://doi.org/10.1021/acs.jmedchem.6c01030
J. Med. Chem. XXXX, XXX, XXX−XXX

2,5-Dioxopyrrolidin-1-yl (3-chloro-4-((1-(2-hydroxy-3-methoxyphenyl)-5-oxo-[1,2,4]triazolo[4,3-*a*]quinazolin-4(5*H*)-yl)methyl)benzoyl)-L-prolinate (26). SHP844 (**24**, 51 mg, 0.088 mmol, 1.0 eq.), *N*,*N*′-dicyclohexylcarbodiimide (22 mg, 0.106 mmol, 1.2 eq.), and *N*-hydroxysuccinimide (12 mg, 0.106 mmol, 1.2 eq.) were dissolved in anhydrous tetrahydrofuran (5 mL). The reaction mixture was stirred at room temperature for 24 h. Then, the mixture was concentrated, and the crude product was purified by normal-phase flash chromatography using dichloromethane and methanol as eluents. Yield: 0.044 g (75%), white crystals. mp 234 °C (dichloromethane/methanol). ^{1}H NMR (300 MHz, $CDCl_3$): δ 8.38 (dd, J = 7.8, 1.7 Hz, 1H), 7.65 (s, 1H), 7.55 (t, J = 6.9 Hz, 1H), 7.46 (t, J = 7.2 Hz, 1H), 7.40−7.30 (m, 2H), 7.28−7.14 (m, 2H), 7.13−7.01 (m, 2H), 5.72 (s, 2H), 4.93 (dd, J = 8.4, 5.0 Hz, 1H), 3.96 (s, 3H), 3.69−3.52 (m, 2H), 2.81 (s, 4H), 2.46−2.26 (m, 2H), 2.18−1.91 (m, 2H). HRMS (ESI$^+$) m/z: [M + H]$^+$, calcd for $C_{33}H_{28}ClN_6O_8$, 671.1651; found, 671.1669. Purity by HPLC: 100%.

Perfluorophenyl (3-Chloro-4-((1-(2-hydroxy-3-methoxyphenyl)-5-oxo-[1,2,4]triazolo[4,3-*a*]quinazolin-4(5*H*)-yl)methyl)benzoyl)-L-prolinate (27). SHP844 (**24**, 20.1 mg, 0.035 mmol, 1.0 eq.), *N*,*N*′-dicyclohexylcarbodiimide (7.9 mg, 0.039 mmol, 1.1 eq.), and pentafluorophenol (7.1 mg, 0.039 mmol, 1.1 eq.) were dissolved in anhydrous tetrahydrofuran (2.5 mL). The reaction mixture was stirred at room temperature for 1 h. The crude reaction mixture was purified directly by preparative reversed phase HPLC using water and acetonitrile as eluents. Yield: 0.010 g (39%), white crystals, mp 227 °C (water/acetonitrile). ^{1}H NMR (500 MHz, THF-d_8): δ 9.23 (t, J = 8.2 Hz, 1H), 8.47 (dd, J = 15.1, 7.8 Hz, 2H), 8.39−8.30 (m, 2H), 8.30−8.24 (m, 2H), 8.19−8.07 (m, 2H), 8.02−7.96 (m, 1H), 7.91−7.83 (m, 1H), 6.57 (d, J = 17.4 Hz, 2H), 4.83 (d, J = 9.2 Hz, 3H), 4.67−4.58 (m, 2H), 3.13−2.91 (m, 2H), 2.33−2.29 (m, 2H), 2.24−2.17 (m, 2H). HRMS (ESI$^+$) m/z [M + H]$^+$, calcd for $C_{35}H_{24}ClF_5N_5O_6$: 740.1329; found, 740.1349. Purity by HPLC: 100%.

Phenyl (3-Chloro-4-((1-(2-hydroxy-3-methoxyphenyl)-5-oxo-[1,2,4]triazolo[4,3-*a*]quinazolin-4(5*H*)-yl)methyl)benzoyl)-L-prolinate (28). SHP844 (**24**, 40.2 mg, 0.070 mmol, 1.0 eq.), was dissolved in DCM (4.0 mL). HATU (26.6 mg, 0.070 mmol, 1.0 eq.), DIPEA (24.0 μL, 0.140 mmol, 2.0 eq.), and phenol (9.9 mg, 0.105 mmol, 1.5 eq.) were added, and the reaction mixture was stirred at room temperature for 16 h. It was concentrated, the residue was redissolved in DMSO (2.0 mL), and it was purified directly by preparative reversed-phase HPLC using water and acetonitrile as eluents. Yield: 0.011 g (24%), white crystals, mp 223 °C (water/acetonitrile). ^{1}H NMR (300 MHz, DMSO-d_6): δ 8.21 (t, J = 6.2 Hz, 1H), 7.72−7.57 (m, 2H), 7.59−7.46 (m, 1H), 7.48−7.20 (m, 7H), 7.09 (dd, J = 13.9, 7.4 Hz, 3H), 6.97−6.90 (m, 1H), 6.77−6.65 (m, 1H), 5.50 (s, 2H), 4.69−4.60 (m, 1H), 3.80 (s, 3H), 2.46−2.32 (m, 2H), 2.10 (dd, J = 15.8, 9.3 Hz, 2H), 2.01−1.87 (m, 2H). HRMS (ESI$^+$) m/z: [M + H]$^+$, calcd for $C_{35}H_{29}ClN_5O_6$, 650.1801; found, 650.1833. Purity by HPLC: 100%.

Pyridin-3-yl (3-Chloro-4-((1-(2-hydroxy-3-methoxyphenyl)-5-oxo-[1,2,4]triazolo[4,3-*a*]quinazolin-4(5*H*)-yl)methyl)benzoyl)-L-prolinate (29). SHP844 (**24**, 40.2 mg, 0.070 mmol, 1.0 eq.), was dissolved in DCM (4.0 mL). HATU (26.6 mg, 0.070 mmol, 1.0 eq.), DIPEA (24.0 μL, 0.140 mmol, 2.0 eq.), and 3-hydroxypyridine (10.0 mg, 0.105 mmol, 1.5 eq.) were added, and the reaction mixture was stirred at room temperature for 16 h. It was concentrated, the residue was redissolved in DMSO (2.0 mL), and it was purified directly by preparative reversed-phase HPLC using water and acetonitrile as eluents. Yield: 0.010 g (22%), white crystals, mp 226 °C (water/acetonitrile). ^{1}H NMR (300 MHz, DMSO-d_6): δ 8.47 (d, J = 16.7 Hz, 2H), 8.27 (s, 1H), 7.80−7.44 (m, 6H), 7.39−7.18 (m, 3H), 7.15−6.81 (m, 2H), 5.53 (s, 2H), 4.72 (s, 2H), 3.87 (s, 3H), 3.71−3.59 (m, 2H), 2.33−2.13 (m, 2H), 2.07−1.86 (m, 2H). HRMS (ESI$^+$) m/z: [M + H]$^+$, calcd for $C_{34}H_{28}ClN_6O_6$, 651.1753; found, 651.1723. Purity by HPLC: 100%.

2,5-Dioxopyrrolidin-1-yl (3-Chloro-4-((1-(2-hydroxy-3-methoxyphenyl)-5-oxo-[1,2,4]triazolo[4,3-*a*]quinazolin-4(5*H*)-yl)methyl)benzoyl)-D-prolinate (30). Compound **25** (25.8 mg, 0.045 mmol, 1.0 eq.), *N*,*N*′-dicyclohexylcarbodiimide (11.1 mg, 0.054 mmol, 1.2 eq.), and *N*-hydroxysuccinimide (6.2 mg, 0.054 mmol, 1.2 eq.) were dissolved in anhydrous tetrahydrofuran (3 mL). The reaction mixture was stirred at room temperature for 3 h. Then, the mixture was concentrated, and the crude product was purified by preparative reversed-phase HPLC using water and acetonitrile as eluents. Yield: 0.009 g (30%), white crystals, mp 233 °C (water/acetonitrile). ^{1}H NMR (500 MHz, DMSO-d_6): δ 8.30−8.20 (m, 1H), 7.59 (dd, J = 14.5, 8.3 Hz, 2H), 7.54 (dd, J = 12.9, 7.3 Hz, 1H), 7.35 (d, J = 8.1 Hz, 1H), 7.29 (d, J = 7.8 Hz, 1H), 7.24−6.98 (m, 4H), 5.58 (d, J = 7.9 Hz, 2H), 5.52−5.47 (m, 1H), 3.91−3.88 (m, 3H), 3.51−3.44 (m, 2H), 2.59 (s, 4H), 1.77−1.71 (m, 2H), 1.64−1.60 (m, 2H). HRMS (ESI$^+$) m/z: [M + H]$^+$, calcd for $C_{33}H_{28}ClN_6O_8$, 671.1651; found, 671.1618. Purity by HPLC: 100%.

2,5-Dioxopyrrolidin-1-yl 3-chloro-4-((1-(2-hydroxy-3-methoxyphenyl)-5-oxo-[1,2,4]triazolo[4,3-*a*]quinazolin-4(5*H*)-yl)methyl)benzoate (31). Benzoic acid derivative **23** (130 mg, 0.27 mmol, 1.0 eq.), *N*,*N*′-dicyclohexylcarbodiimide (68 mg, 0.32 mmol, 1.2 eq.), and *N*-hydroxysuccinimide (38 mg, 0.32 mmol, 1.2 eq.) were dissolved in anhydrous tetrahydrofuran (5 mL). The reaction mixture was stirred at room temperature for 24 h. Upon completion, the mixture was concentrated, and the crude product was purified by normal-phase flash chromatography using dichloromethane and methanol as eluents. Yield: 0.132 g (85%), white crystals. mp 210 °C (dichloromethane/methanol). ^{1}H NMR (300 MHz, DMSO-d_6): δ 9.75 (s, 1H), 8.23−8.17 (m, 2H), 8.05 (dd, J = 8.1, 1.8 Hz, 1H), 7.68 (d, J = 8.2 Hz, 1H), 7.63−7.51 (m, 2H), 7.32 (dd, J = 8.1, 1.6 Hz, 1H), 7.12 (t, J = 7.8 Hz, 2H), 7.03 (t, J = 7.9 Hz, 1H), 5.61 (s, 2H), 3.89 (s, 3H), 2.90 (s, 4H). ^{13}C NMR (75 MHz, DMSO-d_6): δ 172.7, 170.1, 166.1, 160.5, 150.3, 148.0, 146.1, 141.8, 140.5, 134.1, 133.3, 132.9, 130.8, 130.5, 128.9, 128.4, 127.1, 125.7, 122.6, 120.0, 119.1, 115.3, 114.9, 114.2, 56.1, 47.1, 25.5, 25.2. HRMS (ESI$^+$) m/z: [M + H]$^+$, calcd for $C_{28}H_{21}ClN_5O_7$, 574.1124; found, 574.1137. Purity by HPLC: 100%.

***N*-[(3-Aminophenyl)methyl]-3-chloro-4-{[1-(2-hydroxy-3-methoxyphenyl)-5-oxo-4*H*,5*H*-[1,2,4]triazolo[4,3-*a*]quinazolin-4-yl]methyl}benzamide (32).** NHS ester derivative **31** (126 mg, 0.22 mmol, 1.0 eq.) was dissolved in THF (5.0 mL). DIPEA (84 μL, 0.48 mmol, 2.2 eq.) and 3-aminobenzylamine (40 mg, 0.33 mmol, 1.5 eq.) were added. The mixture was stirred at room temperature for 2 h. The reaction mixture was filtered and washed with THF (4.0 mL). The filtrate was concentrated and subjected to reversed-phase flash column chromatography using water and acetonitrile as eluents. Yield: 0.082 g (64%), white powder, mp 257−277 °C (water/acetonitrile). ^{1}H NMR (300 MHz, DMSO-d_6): δ 9.08 (d, J = 5.6 Hz, 1H), 8.27 (d, J = 7.7 Hz, 1H), 8.07 (s, 1H), 7.83−7.69 (m, 2H), 7.56 (t, J = 7.6 Hz, 1H), 7.36 (d, J = 8.1 Hz, 1H), 7.25 (dd, J = 16.3, 7.5 Hz, 2H), 7.07−6.89 (m, 3H), 6.51−6.36 (m, 3H), 5.48 (s, 2H), 5.01 (s, 2H), 4.34 (d, J = 5.5 Hz, 2H), 3.90 (s, 3H). ^{13}C NMR (75 MHz, DMSO-d_6): δ 164.39, 158.38, 148.69, 148.22, 148.08, 146.14, 145.80, 139.84, 136.08, 135.10, 134.98, 134.07, 131.75, 129.05, 128.73, 128.06, 127.51, 126.70, 126.29, 122.77, 119.50, 116.80, 116.15, 115.27, 114.55, 112.37, 112.35, 56.04, 43.96, 42.73. HRMS (ESI$^+$) m/z: [M + H]$^+$, calcd for $C_{31}H_{26}N_6O_4Cl$, 581.1698; found, 581.1715. Purity by HPLC: 99%.

***N*-(2-Aminoethyl)-3-chloro-4-((1-(2-hydroxy-3-methoxyphenyl)-5-oxo-[1,2,4]triazolo[4,3-*a*]quinazolin-4(5*H*)-yl)methyl)benzamide (33).** To a solution of **31** (200 mg, 0.35 mmol, 1.0 eq.) in MeCN (350 μL) was added $NH_2CH_2CH_2NH_2$ (70 μL, 1.04 mmol, 3.0 eq.) the solution was stirred at room temperature for 0.5 h. The solvents were then removed and the residue was submitted to reverse-phase flash chromatography (MeCN and H_2O eluents with 0.1% formic acid), but could not be perfectly purified, so it was taken forward to the next step.

3-Chloro-*N*-({3-[(4,6-dichloro-1,3,5-triazin-2-yl)amino]phenyl}methyl)-4-{[1-(2-hydroxy-3-methoxyphenyl)-5-oxo-4*H*,5*H*-[1,2,4]triazolo[4,3-*a*]quinazolin-4-yl]methyl}benzamide (34). Amine (**32**, 40 mg, 0.07 mmol, 1.0 eq.) was dissolved in abs. THF (4.0 mL), and it was cooled to 0 °C. 1,3,5-Trichlorotriazine (13 mg, 0.07 mmol, 1.0 eq.) was added, and the mixture was stirred at room

https://doi.org/10.1021/acs.jmedchem.6c01030
J. Med. Chem. XXXX, XXX, XXX−XXX

temperature for 1 h. It was filtered and washed with water (2 × 4 mL). Yield: 0.030 g (59%), light yellow powder, mp 197−199 °C (water). ^{1}H NMR (300 MHz, DMSO-d_6): δ 11.11 (s, 1H), 9.22 (t, J = 5.8 Hz, 1H), 8.27 (dd, J = 7.8, 1.2 Hz, 1H), 8.08 (d, J = 1.4 Hz, 1H), 7.82−7.69 (m, 2H), 7.60−7.51 (m, 3H), 7.39−7.27 (m, 3H), 7.21 (d, J = 8.4 Hz, 1H), 7.13 (d, J = 7.7 Hz, 1H), 7.08−6.97 (m, 2H), 5.53 (s, 2H), 4.49 (d, J = 5.7 Hz, 2H), 3.91 (s, 3H). ^{13}C NMR (75 MHz, DMSO-d_6): δ 164.60, 163.73, 158.50, 158.34, 154.08, 148.24, 147.96, 145.75, 145.63, 140.33, 140.24, 136.99, 136.16, 135.00, 134.94, 134.01, 131.80, 131.74, 129.08, 128.86, 128.08, 127.58, 126.77, 126.30, 123.73, 123.30, 122.75, 119.97, 119.80, 116.83, 115.99, 115.23, 114.63, 56.07, 43.98, 42.57. HRMS (ESI$^+$) m/z: [M + H]$^+$, calcd for $C_{34}H_{25}N_9O_4Cl_3$, 728.1089; found, 728.1121. Purity by HPLC: 98%.

3-Chloro-*N*-(2-((4,6-dichloro-1,3,5-triazin-2-yl)amino)ethyl)-4-((1-(2-hydroxy-3-methoxyphenyl)-5-oxo-[1,2,4]triazolo[4,3-*a*]quinazolin-4(5*H*)-yl)methyl)benzamide (35). 1,3,5-Trichlorotriazine (12 mg, 0.066 mmol, 1.1 eq.) was added at 0 °C to a solution of **33** (30 mg, 0.06 mmol) in THF (15 mL). The reaction was stirred at room temperature overnight. The solvent was removed and the crude was purified by reverse-phase flash chromatography (MeCN and H_2O eluents with 0.1% formic acid). Yield: 0.015 g (37%), white solid. ^{1}H NMR (500 MHz, DMSO-d_6): δ 9.02−8.71 (m, 2H), 8.48 (br s, 1H), 8.27 (d, J = 7.8 Hz, 1H), 7.98 (s, 1H), 7.80−7.66 (m, 2H), 7.64−7.53 (m, 1H), 7.46−7.33 (m, 1H), 7.27 (d, J = 7.8 Hz, 1H), 7.23 (d, J = 8.5 Hz, 1H), 7.05 (d, J = 7.2 Hz, 1H), 7.03−6.98 (m, 1H), 5.53 (s, 2H), 4.26 (s, 1H), 4.14 (s, 1H), 3.90 (s, 3H), 3.79 (s, 1H), 3.63 (s, 1H) ppm. ^{13}C NMR (126 MHz, DMSO-d_6): δ 158.85, 156.13, 149.21, 148.68, 148.61, 146.31, 144.44, 136.56, 135.65, 135.56, 135.44, 134.55, 132.17, 129.52, 128.49, 127.95, 127.16, 126.70, 123.49, 123.28, 117.26, 116.64, 115.76, 115.06, 103.38, 60.33, 56.53, 44.41 ppm. HRMS (ESI$^+$) m/z: [M + H]$^+$, calcd for $C_{29}H_{23}N_9O_4Cl_3$, 666.0933; found, 666.0944. Purity by HPLC: 100%.

3-Chloro-4-((1-(2-hydroxy-3-methoxyphenyl)-5-oxo-[1,2,4]triazolo[4,3-*a*]quinazolin-4(5*H*)-yl)methyl)benzohydrazide (36). To a solution of ester **22** (229 mg, 0.47 mmol, 1.0 eq.) in 1,4-dioxane (940 μl), NH_2NH_2 solution in H_2O was added (55%, 128 μl, 1.41 mmol, 3.0 eq.). The mixture was heated in a microwave reactor at 150 °C for 20 min. The solvents were then removed and the residue was purified by reverse-phase chromatography using water + 0.1% HCOOH and acetonitrile + 0.1% HCOOH as eluents. Yield: 149 mg (65%), white-grey solid. ^{1}H NMR (300 MHz, DMSO-d_6): δ 9.90 (s, 1H), 8.27 (d, J = 7.7 Hz, 1H), 7.96 (d, J = 4.3 Hz, 1H), 7.78−7.61 (m, 2H), 7.56 (t, J = 7.6 Hz, 1H), 7.31 (dd, J = 15.3, 7.7 Hz, 2H), 7.21 (d, J = 8.2 Hz, 1H), 7.03 (d, J = 7.6 Hz, 2H), 5.51 (s, 2H), 3.90 (d, J = 4.0 Hz, 3H). ^{13}C NMR (126 MHz, DMSO-d_6): δ 164.12, 158.32, 148.09, 145.72, 135.91, 134.93, 133.99, 131.73, 129.01, 127.75, 127.45, 126.65, 125.77, 122.74, 119.70, 116.13, 115.18, 114.59, 56.04, 43.90. HRMS (ESI$^+$) m/z [M + H]$^+$, calcd for $C_{24}H_{20}N_6O_4Cl$ 491.1229; found, 491.1236. Purity by HPLC: 100%.

3-Chloro-*N*′-(4,6-dichloro-1,3,5-triazin-2-yl)-4-((1-(2-hydroxy-3-methoxyphenyl)-5-oxo-[1,2,4]triazolo[4,3-*a*]quinazolin-4(5*H*)-yl)methyl)benzohydrazide (37). To a solution of **36** (100 mg, 0.20 mmol, 1 eq.) in THF (1 mL), 2,4,6-trichloro-1,3,5-triazine (37 mg, 0.20 mmol, 1 eq.) was added and the mixture was stirred at room temperature for 30 min. THF was then removed and the product purified by reverse-phase chromatography using water + 0.1% HCOOH and acetonitrile + 0.1% HCOOH as eluents. Yield: 64 mg (50%), grey solid. ^{1}H NMR (600 MHz, DMSO-d_6): δ 9.59 (s, 1H), 9.50 (s, 1H), 8.31−8.23 (m, 1H), 8.15 (d, J = 10.8 Hz, 2H), 7.79 (dd, J = 8.1, 1.8 Hz, 1H), 7.74 (ddd, J = 8.8, 7.3, 1.7 Hz, 1H), 7.57 (t, J = 7.5 Hz, 1H), 7.46 (d, J = 8.1 Hz, 1H), 7.29 (dd, J = 7.8, 2.0 Hz, 1H), 7.20 (d, J = 8.5 Hz, 1H), 7.08−7.00 (m, 2H), 5.56 (s, 2H), 3.90 (s, 3H). ^{13}C NMR (151 MHz, DMSO-d_6): δ 163.47, 158.83, 148.54 (d, J = 40.4 Hz), 146.15 (d, J = 14.5 Hz), 137.99, 135.46, 134.51, 132.32 (d, J = 49.5 Hz), 129.48 (d, J = 20.6 Hz), 128.18, 127.38 (d, J = 60.4 Hz), 123.33 (d, J = 32.6 Hz) 120.24, 117.28, 116.59, 115.35 (d, J = 94.7 Hz), 56.52, 44.45. HRMS (ESI$^+$) m/z: [M + H]$^+$, calcd for $C_{27}H_{19}N_9O_4Cl_3$, 638.0620; found, 638.0618. Purity by HPLC: 100%.

■ ASSOCIATED CONTENT

Supporting Information

The Supporting Information is available free of charge at https://pubs.acs.org/doi/10.1021/acs.jmedchem.6c01030.

Supporting Information contains structure and characterization of the mapping library, mapping of SHP2, stability data, further predicted binding modes of designed compounds, materials and methods, experimental procedures, computational methods, X-ray data, dose−response curves, intact MS spectra, digestion data, compound characterization, NMR spectra, HRMS spectra, HPLC traces (PDF)

In separate files molecular formula strings (CSV)

SHP2—26 crystal structure (PDB)

■ AUTHOR INFORMATION

Corresponding Authors

Péter Ábrányi-Balogh − *Medicinal Chemistry Research Group, HUN-REN Research Centre for Natural Sciences, 1117 Budapest, Hungary; Department of Organic Chemistry and Technology, Faculty of Chemical Technology and Biotechnology, Budapest University of Technology and Economics, H-1111 Budapest, Hungary; National Drug Research and Development Laboratory, HUN-REN Research Centre for Natural Sciences, 1117 Budapest, Hungary;* orcid.org/0000-0002-9284-5160; Email: abranyi-balogh.peter@ttk.hu

György M. Keserű − *Medicinal Chemistry Research Group, HUN-REN Research Centre for Natural Sciences, 1117 Budapest, Hungary; Department of Organic Chemistry and Technology, Faculty of Chemical Technology and Biotechnology, Budapest University of Technology and Economics, H-1111 Budapest, Hungary; National Drug Research and Development Laboratory, HUN-REN Research Centre for Natural Sciences, 1117 Budapest, Hungary;* orcid.org/0000-0003-1039-7809; Email: keseru.gyorgy@ttk.hu

Authors

Vincenzo Di Lorenzo − *Medicinal Chemistry Research Group, HUN-REN Research Centre for Natural Sciences, 1117 Budapest, Hungary; Department of Organic Chemistry and Technology, Faculty of Chemical Technology and Biotechnology, Budapest University of Technology and Economics, H-1111 Budapest, Hungary; National Drug Research and Development Laboratory, HUN-REN Research Centre for Natural Sciences, 1117 Budapest, Hungary;* orcid.org/0000-0002-3140-3561

Noémi Csorba − *Medicinal Chemistry Research Group, HUN-REN Research Centre for Natural Sciences, 1117 Budapest, Hungary; Department of Organic Chemistry and Technology, Faculty of Chemical Technology and Biotechnology, Budapest University of Technology and Economics, H-1111 Budapest, Hungary; National Drug Research and Development Laboratory, HUN-REN Research Centre for Natural Sciences, 1117 Budapest, Hungary*

Renáta Szabó − *Medicinal Chemistry Research Group, HUN-REN Research Centre for Natural Sciences, 1117 Budapest, Hungary; Department of Organic Chemistry and Technology, Faculty of Chemical Technology and*

Biotechnology, Budapest University of Technology and Economics, H-1111 Budapest, Hungary; National Drug Research and Development Laboratory, HUN-REN Research Centre for Natural Sciences, 1117 Budapest, Hungary

Levente Kollár − *Medicinal Chemistry Research Group, HUN-REN Research Centre for Natural Sciences, 1117 Budapest, Hungary; National Drug Research and Development Laboratory, HUN-REN Research Centre for Natural Sciences, 1117 Budapest, Hungary;* orcid.org/0000-0001-9679-3735

Yvette Roske − *Structural Biology, Max-Delbruck-Center for Molecular Medicine in the Helmholtz Association (MDC), 13125 Berlin, Germany*

Ivan Ranđelović − *Department of Experimental Pharmacology and the National Tumor Biology Laboratory, National Institute of Oncology, 1122 Budapest, Hungary*

Krisztina Balázs − *Medicinal Chemistry Research Group, HUN-REN Research Centre for Natural Sciences, 1117 Budapest, Hungary; National Drug Research and Development Laboratory, HUN-REN Research Centre for Natural Sciences, 1117 Budapest, Hungary*

Tibor Viktor Szalai − *Medicinal Chemistry Research Group, HUN-REN Research Centre for Natural Sciences, 1117 Budapest, Hungary; National Drug Research and Development Laboratory, HUN-REN Research Centre for Natural Sciences, 1117 Budapest, Hungary; Department of Inorganic and Analytical Chemistry, Faculty of Chemical Technology and Biotechnology, Budapest University of Technology and Economics, H-1111 Budapest, Hungary;* orcid.org/0009-0000-4088-3117

Nina-Louisa Efrém − *Leibniz-Forschungsinstitut fur Molekulare Pharmakologie (FMP), 13125 Berlin, Germany; Institute of Organic Chemistry, Organic Chemistry I, Karlsruhe Institute of Technology, 76131 Karlsruhe, Germany;* orcid.org/0009-0000-6505-4120

Levente Mihalovits − *Medicinal Chemistry Research Group, HUN-REN Research Centre for Natural Sciences, 1117 Budapest, Hungary; National Drug Research and Development Laboratory, HUN-REN Research Centre for Natural Sciences, 1117 Budapest, Hungary*

Tímea Imre − *Medicinal Chemistry Research Group, HUN-REN Research Centre for Natural Sciences, 1117 Budapest, Hungary; National Drug Research and Development Laboratory, HUN-REN Research Centre for Natural Sciences, 1117 Budapest, Hungary; MS Metabolomics Research Group, HUN-REN Research Centre for Natural Sciences, 1117 Budapest, Hungary*

József Simon − *Medicinal Chemistry Research Group, HUN-REN Research Centre for Natural Sciences, 1117 Budapest, Hungary; National Drug Research and Development Laboratory, HUN-REN Research Centre for Natural Sciences, 1117 Budapest, Hungary; MS Metabolomics Research Group, HUN-REN Research Centre for Natural Sciences, 1117 Budapest, Hungary*

József Tóvári − *Department of Experimental Pharmacology and the National Tumor Biology Laboratory, National Institute of Oncology, 1122 Budapest, Hungary*

Marc Nazaré − *Leibniz-Forschungsinstitut fur Molekulare Pharmakologie (FMP), 13125 Berlin, Germany; Department of Chemistry, Organic and Bioorganic Chemistry, Bielefeld University, 33615 Bielefeld, Germany;* orcid.org/0000-0002-1602-2330

Oliver Daumke − *Structural Biology, Max-Delbruck-Center for Molecular Medicine in the Helmholtz Association (MDC), 13125 Berlin, Germany; Leibniz-Forschungsinstitut fur Molekulare Pharmakologie (FMP), 13125 Berlin, Germany*

Complete contact information is available at: https://pubs.acs.org/doi/10.1021/acs.jmedchem.6c01030

Author Contributions

V.D.L., L.K., R.S., K.B., and P.Á.-B. designed, synthesized and characterized the compounds. N.C. compiled the fragment library, set and measured the biochemical assay, measured protein MS and contributed to manuscript writing. T.I. and J.S. measured protein MS, performed enzymatic digestions and MS/MS measurements. T.V.S. and L.M. have performed molecular docking studies. Y.R. purified and crystallized the SHP2 constructs with compound **26**, determined its structure, provided structural comparisons and contributed to writing. N.L.-E contributed to the investigation and formal analysis. O. D. participated in funding and contributed to writing. M.N. contributed to funding and conceptualization. P.Á.-B. supervised the work, wrote and edited the manuscript. G.M.K. conceptualized and supervised the project, provided funding and wrote the manuscript.

Notes

The authors declare no competing financial interest.

■ ACKNOWLEDGMENTS

The authors received funding from the MSCA ITN "ALLODD" [grant no. 956314 to G.M.K.], the National Research Development and Innovation Office of Hungary [PharmaLab (RRF-2.3.1-21-2022-00015) to G.M.K. and NKFIH-OTKA K147410 to J.T.] and the Schweizerische Nationalfonds (SNF) [MAPS 230109]. P.Á.-B. was supported by the János Bolyai Research Scholarship of the Hungarian Academy of Sciences. Sz.R. and G.M.K. was supported by project C2246513, KDP-IKT-2023-900-I1-00000957/0000003 provided by the Ministry of Culture and Innovation of Hungary from the National Research, Development and Innovation fund, financed under the KDP-2023 funding scheme. Authors are grateful for András György Németh for his contribution in syntheses and László Petri and Zoltán Szabó for MS measurements. We acknowledge the HPC time and support of the Governmental Information Technology Development Agency, Hungary.

■ ABBREVIATIONS

DiFMUP, 6,8-difluoro-4-methylumbelliferyl phosphate; EPIC-Fit, enzyme preincubation IC_{50} fitting method; HPLC−MS, high-performance liquid chromatography−mass spectrometry; IC_{50}, half-maximum inhibitory concentration; IRS-1, insulin receptor substrate 1; K_I, equilibrium inhibition constant; k_{inact}, maximal rate constant for covalent inactivation; k_{Lys}, pseudo-first-order rate constants for lysine modification; LC−MS/MS, liquid chromatography−tandem mass spectrometry; MCS-RMSD, maximum common substructure root-mean-square deviation; MS, mass spectrometry; NASA, *N*-alkyl-*N*-aryl sulfonamide; NHS, *N*-hydroxysuccinimide; PDB, Protein Data Bank; PTP, protein tyrosine phosphatase; SAR, structure−activity relationship; SASA, solvent accessible surface area;

SH2, Src homology 2 domain; SHP2, Src homology 2−containing protein tyrosine phosphatase 2; SHP2FL, full-length SHP2; S_NAr, nucleophilic aromatic substitution; TCI, targeted covalent inhibitor; TIPS, triisopropylsilyl.

REFERENCES

(1) Asmamaw, M. D.; Shi, X. J.; Zhang, L. R.; Liu, H. M. A Comprehensive Review of SHP2 and Its Role in Cancer. *Cell. Oncol.* **2022**, *45* (5), 729−753.

(2) Chen, X.; Keller, S. J.; Hafner, P.; Alrawashdeh, A. Y.; Avery, T. Y.; Norona, J.; Zhou, J.; Ruess, D. A. Tyrosine Phosphatase PTPN11/SHP2 in Solid Tumors - Bull's Eye for Targeted Therapy? *Front. Immunol.* **2024**, *15*, 1340726.

(3) Welsh, C. L.; Allen, S.; Madan, L. K. Setting Sail: Maneuvering SHP2 Activity and Its Effects in Cancer. *Adv. Cancer Res.* **2023**, *160*, 17.

(4) Chen, Y. N. P.; Lamarche, M. J.; Chan, H. M.; Fekkes, P.; Garcia-Fortanet, J.; Acker, M. G.; Antonakos, B.; Chen, C. H. T.; Chen, Z.; Cooke, V. G.; Dobson, J. R.; Deng, Z.; Fei, F.; Firestone, B.; Fodor, M.; Fridrich, C.; Gao, H.; Grunenfelder, D.; Hao, H. X.; Jacob, J.; Ho, S.; Hsiao, K.; Kang, Z. B.; Karki, R.; Kato, M.; Larrow, J.; La Bonte, L. R.; Lenoir, F.; Liu, G.; Liu, S.; Majumdar, D.; Meyer, M. J.; Palermo, M.; Perez, L.; Pu, M.; Price, E.; Quinn, C.; Shakya, S.; Shultz, M. D.; Slisz, J.; Venkatesan, K.; Wang, P.; Warmuth, M.; Williams, S.; Yang, G.; Yuan, J.; Zhang, J. H.; Zhu, P.; Ramsey, T.; Keen, N. J.; Sellers, W. R.; Stams, T.; Fortin, P. D. Allosteric Inhibition of SHP2 Phosphatase Inhibits Cancers Driven by Receptor Tyrosine Kinases. *Nature* **2016**, *535* (7610), 148−152.

(5) Liu, M.; Gao, S.; Elhassan, R. M.; Hou, X.; Fang, H. Strategies to Overcome Drug Resistance Using SHP2 Inhibitors. *Acta Pharm. Sin. B* **2021**, *11* (12), 3908−3924.

(6) Kerr, D. L.; Haderk, F.; Bivona, T. G. Allosteric SHP2 Inhibitors in Cancer: Targeting the Intersection of RAS, Resistance, and the Immune Microenvironment. *Curr. Opin. Chem. Biol.* **2021**, *62*, 1−12.

(7) Song, Y.; Yang, X.; Wang, S.; Zhao, M.; Yu, B. Crystallographic Landscape of SHP2 Provides Molecular Insights for SHP2 Targeted Drug Discovery. *Med. Res. Rev.* **2022**, *42* (5), 1781−1821.

(8) Guo, Z.; Duan, Y.; Sun, K.; Zheng, T.; Liu, J.; Xu, S.; Xu, J. Advances in SHP2 Tunnel Allosteric Inhibitors and Bifunctional Molecules. *Eur. J. Med. Chem.* **2024**, *275*, 116579.

(9) Day, J. E. H.; Berdini, V.; Castro, J.; Chessari, G.; Davies, T. G.; Day, P. J.; St. Denis, J. D.; Fujiwara, H.; Fukaya, S.; Hamlett, C. C. F.; Hearn, K.; Hiscock, S. D.; Holvey, R. S.; Ito, S.; Kandola, N.; Kodama, Y.; Liebeschuetz, J. W.; Martins, V.; Matsuo, K.; Mortenson, P. N.; Muench, S.; Nakatsuru, Y.; Ochiiwa, H.; Palmer, N.; Peakman, T.; Price, A.; Reader, M.; Rees, D. C.; Rich, S. J.; Shah, A.; Shibata, Y.; Smyth, T.; Twigg, D. G.; Wallis, N. G.; Williams, G.; Wilsher, N. E.; Woodhead, A.; Shimamura, T.; Johnson, C. N. Fragment-Based Discovery of Allosteric Inhibitors of SH2 Domain-Containing Protein Tyrosine Phosphatase-2 (SHP2). *J. Med. Chem.* **2024**, *67* (6), 4655−4675.

(10) Kong, J.; Long, Y. Q. Recent Advances in the Discovery of Protein Tyrosine Phosphatase SHP2 Inhibitors. *RSC Med. Chem.* **2022**, *13* (3), 246−257.

(11) Singh, J. The Ascension of Targeted Covalent Inhibitors. *J. Med. Chem.* **2022**, *65* (8), 5886−5901.

(12) Hillebrand, L.; Liang, X. J.; Serafim, R. A. M.; Gehringer, M. Emerging and Re-Emerging Warheads for Targeted Covalent Inhibitors: An Update. *J. Med. Chem.* **2024**, *67*, 7668−7758.

(13) Gai, C.; Harnor, S. J.; Zhang, S.; Cano, C.; Zhuang, C.; Zhao, Q.; Zhuang, C.; Zhao, Q. Advanced Approaches of Developing Targeted Covalent Drugs. *RSC Med. Chem.* **2022**, *13* (12), 1460−1475.

(14) Hameed, M. S.; Cao, H.; Guo, L.; Zeng, L.; Ren, Y. Advancements, Challenges, and Future Frontiers in Covalent Inhibitors and Covalent Drugs: A Review. *Eur. J. Med. Chem. Rep.* **2024**, *12*, 100217.

(15) Zhang, J.; Gao, W.; Wang, Y.; Chang, J.; Yu, B. Targeted Covalent Inhibitors for Novel Therapeutics. *Future Med. Chem.* **2023**, *15* (19), 1739−1741.

(16) Peng, Q.; Weerapana, E. Profiling Nuclear Cysteine Ligandability and Effects on Nuclear Localization Using Proximity Labeling-Coupled Chemoproteomics. *Cell Chem. Biol.* **2024**, *31* (3), 550−564.e9.

(17) Szalai, T. V.; di Lorenzo, V.; Péczka, N.; Mihalovits, L. M.; Petri, L.; Ashraf, Q. F.; de Araujo, E. D.; Honti, V.; Bajusz, D.; Keserű, G. M. Allosteric Covalent Inhibitors of the STAT3 Transcription Factor from Virtual Screening. *ACS Med. Chem. Lett.* **2025**, *16* (6), 991−997.

(18) Brennan, A.; Lovell, S.; Vance, K. W.; Mason, J. M. An Intracellular Peptide Library Screening Platform Identifies Irreversible Covalent Transcription Factor Inhibitors. *Adv. Sci.* **2025**, *12* (18), 2416963.

(19) Kirschner, T.; Müller, MP; Rauh, D. Targeting KRAS Diversity: Covalent Modulation of G12X and Beyond in Cancer Therapy. *J. Med. Chem.* **2024**, *67* (8), 6044−6051.

(20) Orgován, Z.; Péczka, N.; Petri, L.; Ábrányi-Balogh, P.; Randelović, I.; Tóth, S.; Szakács, G.; Nyíri, K.; Vértessy, B.; Pálfy, G.; Vida, I.; Perczel, A.; Tóvári, J.; Keserű, G. M. Covalent Fragment Mapping of KRasG12C Revealed Novel Chemotypes with in Vivo Potency. *Eur. J. Med. Chem.* **2023**, *250*, 115212.

(21) Maciag, A. E.; Yang, Y.; Sharma, A. K.; Turner, D. M.; DeHart, C. J.; Abdelkarim, H.; Fan, L.; Smith, B. P.; Kumari, V.; Dyba, M.; Rigby, M.; Castillo Badillo, J. A.; Adams, L.; Fornelli, L.; Fox, S.; Brafman, A.; Turbyville, T.; Gillette, W.; Messing, S.; Agamasu, C.; Wolfe, A. L.; Gysin, S.; Chan, A. H.; Simanshu, D. K.; Esposito, D.; Chertov, O.; Stephen, A. G.; Arkin, M.; Renslo, A.; Kelleher, N. L.; Gaponenko, V.; Lightstone, F. C.; Nissley, D. V.; McCormick, F. Blocking C-Terminal Processing of KRAS4b via a Direct Covalent Attack on the CaaX-Box Cysteine. *Proc. Natl. Acad. Sci. U.S.A.* **2025**, *122* (19), e2410766122.

(22) Sirocchi, L. S.; Scharnweber, M.; Oberndorfer, S.; Siszler, G.; Zak, K. M.; Rumpel, K.; Neumüller, R. A.; Wilding, B. Discovery of Carbodiimide Warheads to Selectively and Covalently Target Aspartic Acid in KRASG12D. *J. Am. Chem. Soc.* **2025**, *147* (18), 15787−15795.

(23) Martínez-Cartró, M.; Serrano-Morrás, Á.; Bertran-Mostazo, A.; Castaño-Muñiz, R.; Scaffidi, S.; Ivanova, V.; Csorba, N.; Simon, J.; Ábrányi-Balogh, P.; Li, Y.; Keserű, G. M.; Hao, B.; Barril, X.; Galdeano, C. Discovering Uncharted Binding Pockets on E3 Ligases Leads to the Identification of FBW7 Allosteric Modulators. *Adv. Sci.* **2025**, *12* (39), e06068.

(24) Yuan, M.; Chu, Y.; Duan, Y. Reversible Covalent PROTACs: Novel and Efficient Targeted Degradation Strategy. *Front. Chem.* **2021**, *9*, 691093.

(25) Ward, C. C.; Kleinman, J. I.; Brittain, S. M.; Lee, P. S.; Chung, C. Y. S.; Kim, K.; Petri, Y.; Thomas, J. R.; Tallarico, J. A.; McKenna, J. M.; Schirle, M.; Nomura, D. K. Covalent Ligand Screening Uncovers a RNF4 E3 Ligase Recruiter for Targeted Protein Degradation Applications. *ACS Chem. Biol.* **2019**, *14* (11), 2430−2440.

(26) Rodríguez-Gimeno, A.; Galdeano, C. Drug Discovery Approaches to Target E3 Ligases. *ChemBioChem* **2025**, *26* (1), e202400656.

(27) Csorba, N.; Ábrányi-Balogh, P.; Keserű, G. M. Covalent Fragment Approaches Targeting Non-Cysteine Residues. *Trends Pharmacol. Sci.* **2023**, *44* (11), 802−816.

(28) Jones, L. H. Design of Next-Generation Covalent Inhibitors: Targeting Residues beyond Cysteine. *Annual Reports in Medicinal Chemistry*; 1st ed.; Elsevier Inc., 2020; Vol. *56* pp 95−134.

(29) Kim, G.; Grams, R. J.; Hsu, K. L. Advancing Covalent Ligand and Drug Discovery beyond Cysteine. *Chem. Rev.* **2025**, *125* (14), 6653−6684.

(30) Mehta, N. V.; Degani, M. S. The Expanding Repertoire of Covalent Warheads for Drug Discovery. *Drug Discov. Today* **2023**, *28* (12), 103799.

(31) Raouf, Y. S. Covalent Inhibitors: To Infinity and Beyond. *J. Med. Chem.* **2024**, *67* (13), 10513−10516.

(32) Abbasov, M. E.; Kavanagh, M. E.; Ichu, T.-A.; Lazear, M. R.; Tao, Y.; Crowley, V. M.; am Ende, C. W.; Hacker, S. M.; Ho, J.; Dix, M. M.; Suciu, R.; Hayward, M. M.; Kiessling, L. L.; Cravatt, B. F. A Proteome-Wide Atlas of Lysine-Reactive Chemistry. *Nat. Chem.* **2021**, *13* (11), 1081−1092.
(33) Efrém, N.-L.; Csorba, N.; Amoussa, M.; Ábrányi-Balogh, P.; Guo, Z.; Petri, L.; Bo, F.; Di Lorenzo, V.; Roske, Y.; Szalai, T. V.; Mihalovits, L.; Simon, J.; Li, J.; Daumke, O.; Keserű, G. M.; Nazaré, M. Mapping the SHP2 Allosteric Pocket With Target-Biased Covalent Fragments. *ChemBioChem* **2026**, *27* (8), e70310.
(34) Petri, L.; Egyed, A.; Bajusz, D.; Imre, T.; Hetényi, A.; Martinek, T.; Ábrányi-Balogh, P.; Keserű, G. M. An Electrophilic Warhead Library for Mapping the Reactivity and Accessibility of Tractable Cysteines in Protein Kinases. *Eur. J. Med. Chem.* **2020**, *207*, 112836.
(35) Petri, L.; Ábrányi-Balogh, P.; Tímea, I.; Pálfy, G.; Perczel, A.; Knez, D.; Hrast, M.; Gobec, M.; Sosič, I.; Nyiri, K.; Vértessy, B. G.; Jänsch, N.; Desczyk, C.; Meyer-Almes, F. J.; Ogris, I.; Golič Grdadolnik, S.; Iacovino, L. G.; Binda, C.; Gobec, S.; Keserű, G. M. Assessment of Tractable Cysteines for Covalent Targeting by Screening Covalent Fragments. *ChemBioChem* **2020**, *22* (4), 743−753.
(36) Fodor, M.; Price, E.; Wang, P.; Lu, H.; Argintaru, A.; Chen, Z.; Glick, M.; Hao, H. X.; Kato, M.; Koenig, R.; LaRochelle, J. R.; Liu, G.; McNeill, E.; Majumdar, D.; Nishiguchi, G. A.; Perez, L. B.; Paris, G.; Quinn, C. M.; Ramsey, T.; Sendzik, M.; Shultz, M. D.; Williams, S. L.; Stams, T.; Blacklow, S. C.; Acker, M. G.; LaMarche, M. J. Dual Allosteric Inhibition of SHP2 Phosphatase. *ACS Chem. Biol.* **2018**, *13* (3), 647−656.
(37) Ye, W.; Liu, Y.; Ren, Q.; Liao, T.; Chen, Y.; Chen, D.; Wang, S.; Yao, L.; Jia, Y.; Zhao, C.; Zhou, Z. Design, Synthesis and Biological Evaluation of Novel Triazoloquinazolinone and Imidazoquinazolinone Derivatives as Allosteric Inhibitors of SHP2 Phosphatase. *J. Enzyme Inhib. Med. Chem.* **2022**, *37* (1), 1495−1513.
(38) Luo, R.; Wang, Z.; Luo, D.; Qin, Y.; Zhao, C.; Yang, D.; Lu, T.; Zhou, Z.; Huang, Z. Design, Synthesis, and Biological Evaluation of Novel Triazoloquinazolinone Derivatives as SHP2 Protein Inhibitors. *J. Enzyme Inhib. Med. Chem.* **2021**, *36* (1), 2170−2182.
(39) Song, W.; Li, L.; Liao, T.; Chen, D.; Jia, Y.; Zhao, X.; Zheng, Z.; Zhou, Z. S. Crystal Structure, DFT Study, Hirshfeld Surface Analysis, Molecular Docking and Antitumor Activity of a Novel SHP2 Inhibitor. *J. Mol. Struct.* **2024**, *1301*, 137320.
(40) Péczka, N.; Orgován, Z.; Ábrányi-Balogh, P.; Keserű, G. M. Electrophilic Warheads in Covalent Drug Discovery: An Overview. *Expert Opin. Drug Discov.* **2022**, *17* (4), 413−422.
(41) Hacker, S. M.; Backus, K. M.; Lazear, M. R.; Forli, S.; Correia, B. E.; Cravatt, B. F. Global Profiling of Lysine Reactivity and Ligandability in the Human Proteome. *Nat. Chem.* **2017**, *9* (12), 1181−1190.
(42) Lefèbre, J.; Besch, M.; Csorba, N.; Garami, K.; Orgován, Z.; Schlosser, G.; Bermejo, I.; Ábrányi-Balogh, P.; Keserű, G. M.; Rademacher, C. Covalent Activation of the C-Type Lectin DC-SIGN. *Angew. Chem. Int. Ed. Engl.* **2025**, *65* (3), e20594.
(43) Ábrányi-Balogh, P.; Petri, L.; Imre, T.; Szijj, P.; Scarpino, A.; Hrast, M.; Mitrović, A.; Fonovič, U. P.; Németh, K.; Barreteau, H.; Roper, D. I.; Horváti, K.; Ferenczy, G. G.; Kos, J.; Ilaš, J.; Gobec, S.; Keserű, G. M. A Road Map for Prioritizing Warheads for Cysteine Targeting Covalent Inhibitors. *Eur. J. Med. Chem.* **2018**, *160*, 94−107.
(44) Gilbert, K.; Vuorinen, A.; Aatkar, A.; Pogány, P.; Pettinger, J.; Grant, E. K.; Kirkpatrick, J. M.; Rittinger, K.; House, D.; Burley, G. A.; et al. Profiling Sulfur(VI) Fluorides as Reactive Functionalities for Chemical Biology Tools and Expansion of the Ligandable Proteome. *ACS Chem. Biol.* **2023**, *18* (2), 285−295.
(45) Dahal, U. P.; Gilbert, A. M.; Obach, R. S.; Flanagan, M. E.; Chen, J. M.; Garcia-Irizarry, C.; Starr, J. T.; Schuff, B.; Uccello, D. P.; Young, J. A. Intrinsic Reactivity Profile of Electrophilic Moieties to Guide Covalent Drug Design:: N -α-Acetyl-l-Lysine as an Amine Nucleophile. *Medchemcomm* **2016**, *7* (5), 864−872.
(46) Bas, D. C.; Rogers, D. M.; Jensen, J. H. Very Fast Prediction and Rationalization of PKa Values for Protein-Ligand Complexes. *Proteins: Struct. Funct. Bioinf.* **2008**, *73* (3), 765−783.
(47) Olsson, M. H. M.; Søndergaard, C. R.; Rostkowski, M.; Jensen, J. H. PROPKA3: Consistent Treatment of Internal and Surface Residues in Empirical p K a Predictions. *J. Chem. Theory Comput.* **2011**, *7* (2), 525−537.
(48) Søndergaard, C. R.; Olsson, M. H. M.; Rostkowski, M.; Jensen, J. H. Improved Treatment of Ligands and Coupling Effects in Empirical Calculation and Rationalization of pKa Values. *J. Chem. Theory Comput.* **2011**, *7* (7), 2284−2295.
(49) Driowya, M.; Leclercq, J.; Verones, V.; Barczyk, A.; Lecoeur, M.; Renault, N.; Flouquet, N.; Ghinet, A.; Berthelot, P.; Lebegue, N. Synthesis of Triazoloquinazolinone Based Compounds as Tubulin Polymerization Inhibitors and Vascular Disrupting Agents. *Eur. J. Med. Chem.* **2016**, *115*, 393−405.
(50) Wang, Z.; Wang, X.; Li, Y.; Li, P.; Huang, S.; Chen, P.; Tang, G.; Ding, X.; Zhang, Z.; Zhang, Z.-M.; Zhou, Y.; Yao, S. Q.; Lu, X. Cell-Active, Irreversible Covalent Inhibitors Targeting a Surface-Exposed Non-Catalytic Lysine on Aurora a Kinase by Using Squarate Chemistry. *Angew. Chem.* **2025**, *137* (40), e202510763.
(51) Heppner, D. E.; Ogboo, B. C.; Urul, D. A.; May, E. W.; Schaefer, E. M.; Murkin, A. S.; Gehringer, M. Demystifying Functional Parameters for Irreversible Enzyme Inhibitors. *J. Med. Chem.* **2024**, *67* (17), 14693−14696.
(52) Mader, L. K.; Keillor, J. W. Fitting of Kinact and KI Values from Endpoint Pre-Incubation IC50 Data. *ACS Med. Chem. Lett.* **2024**, *15* (5), 731−738.
(53) Zhai, X.; Ward, R. A.; Doig, P.; Argyrou, A. Insight into the Therapeutic Selectivity of the Irreversible EGFR Tyrosine Kinase Inhibitor Osimertinib through Enzyme Kinetic Studies. *Biochemistry* **2020**, *59* (14), 1428−1441.
(54) Case Study - COVALfinder to Study Irreversible EGFR Drugs| Enzymlogic. https://www.enzymlogic.com/resources/covalfinder-the-ideal-tool-for-irreversible-drug-discovery-programs/(accessed 02 27, 2026).